HEAT AND WATER VAPOUR DIFFUSIVITIES NEAR THE BASE OF A DISTURBED STABLE INTERNAL BOUNDARY LAYER

JOHANNES LAUBACH[1], KEITH G. McNAUGHTON[2] and JOHN D. WILSON[3]
[1]*Max-Planck-Institut für Biogeochemie, Postfach 10 01 64, D-07701 Jena, Germany*
[2]*INRA-Bioclimatologie, B. P. 81, F-33883 Villenave d'Ornon Cedex, France*
[3]*University of Alberta, Edmonton, Alberta T6G 2E3, Canada*

(Received in final form 27 July 1999)

Abstract. We present results from an experiment that was designed to investigate turbulent transport relationships in a nearly homogeneous boundary layer disturbed by unsteady wind swings, as found at the base of an advective inversion with a convective boundary layer overhead. In such a situation we measured vertical gradients and eddy fluxes of temperature and humidity at two heights. From these, the turbulent diffusivities of heat and water vapour are obtained, and compared to the predictions of Monin–Obukhov similarity theory and those of a numerical second-order closure model. It is found that the measured diffusivities exceed both predictions. This is interpreted as a consequence of the unsteady conditions. It is also found that the diffusivity for heat is roughly 10% larger than that for water vapour. This is in agreement with a theoretical treatment of the unsteadiness effects that we developed in an earlier publication. This result is not reproduced by the numerical model because the model has no provision for unsteady conditions. Our result disagrees with that from an earlier, very similar, field experiment, which may be due to a systematic underestimation of sensible heat flux in the older experiment.

Keywords: Advection, Disturbed boundary layer, Eddy correlation, Monin–Obukhov similarity theory, Scalar transport, Turbulent diffusion.

1. Introduction

Monin–Obukhov similarity theory (MOST) describes the statistical structure of flow in the atmospheric surface layer over perfectly flat and uniform land, when the conditions overhead are steady. The real world seldom matches the ideal, so much of contemporary research is concerned with extending into more complex situations: concerning itself with flow over topography, with advection and with unsteady forcing of the surface layer. Of these, unsteadiness is remarkable in having received so little attention, even though steady forcing of the surface layer is at least as rare as the occurrence of truly flat or uniform ground. Unsteadiness is the general subject of this paper. More specifically, we deal with the effects of variable wind on the eddy diffusivities for heat and water vapour in a surface layer over flat, uniform ground.

Our understanding of the effects of unsteadiness has changed significantly during our research. The original idea, which dictated our experimental design and

Boundary-Layer Meteorology **94:** 23–63, 2000.

selection of the site, was that slow variations in windspeed would produce short-term variations in momentum transfer, but that turbulence near the ground would maintain a continuous equilibrium so that the statistical relationships of MOST would be obeyed during brief intervals. If so, we reasoned in an earlier paper (McNaughton and Laubach, 1998, henceforth ML98), air temperature and humidity would change with windspeed near the ground, causing changing gradients of temperature and humidity above a crop and changing saturation deficit within the crop canopy. The fluxes of temperature and humidity, changing in step with the saturation deficit, would therefore vary during an observation period (of, say, 20 min) that contained several of the brief 'equilibrium' intervals. ML98 showed results confirming this hypothesis, and argued that the varying fluxes and gradients averaged over whole observation periods could give diffusivities that departed from MOST, even though MOST was obeyed from one brief interval to the next. In particular, they argued that the diffusivity for heat should exceed that for water vapour at the base of an advective inversion over a freely transpiring crop. To verify this last prediction was the original aim of the current paper.

In the event, our experiment produced results that cannot be fully explained by our original hypothesis on the effects of varying winds on scalar diffusivities. In particular, spectral analysis of the data shows that the fluxes of all scalars are enhanced in a disturbed surface layer near the ground, when compared against results from homogeneous undisturbed surface layers. The spectra are presented in a companion paper (McNaughton and Laubach, 2000). The exact mechanism is not yet clear, though updrafts and downdrafts associated with changing windspeed and direction may be important. We develop some ideas in the companion paper. Whatever the cause, the signature of the mechanism is enhanced vertical scalar flux at low frequencies. This observation suggests that the scalar diffusivities should be larger than predicted by MOST in a disturbed surface layer. In other words, we find evidence that unsteadiness plays an 'active' role in scalar transport. In ML98 we used this term in the same sense as Townsend (1961). It seems that the enhancement of transport at low frequencies is similar for all scalars, regardless of how they are released at the ground surface. If so, then this does not affect the ratio of the diffusivities for heat and water vapour, unlike the mechanism described in the previous paragraph. This prediction also remains to be verified.

Thus, the purpose of this paper is to present results from our analysis of the eddy diffusivities that verify the above predictions. Because this puts high demands on measurement accuracy, we provide a detailed description of the site and instrumentation (Section 4) and an extensive error assessment (Section 5).

Although our objective was to study one-dimensional transport processes, we chose to make our measurements at the base of an advective inversion formed over a paddy field downwind of an arid region, albeit with as large a fetch as possible over the crop. This was to obtain the optimum conditions of large vertical gradients of saturation deficit over a freely transpiring crop, and of variable wind overhead. The disadvantage of this site was that we inevitably ran the risk of having the

effects of unsteadiness confounded with the effects of advection in our results. In order to assess the latter, we present the vertical divergences of the observed fluxes of momentum and scalars, and we give comparisons of our experimental data with results from a numerical turbulence model for advection, closed at second order. It turns out that advection should have had little effect on our resulting diffusivities. It is therefore justified to consider our experiment as a successful test of the predictions of ML98.

In this context it should be noted that our new understanding of the unsteadiness phenomena, as outlined above, has changed our initial judgment of data quality, too. In ML98 we formulated: 'early analysis ... shows evidence that the lowest instrument level used was not in the fully adjusted layer'. This statement was mainly based on the observation that our spectra resembled those reported from other advection experiments (Lang et al., 1983; Zermeño-González and Hipps, 1997). We have revised our interpretation of such spectral behaviour and consider it now as a characteristic of disturbance, not advection. This is fully discussed in McNaughton and Laubach (2000).

2. Mechanisms for Unequal Diffusivities of Scalar Variables

2.1. Definition and MOST prediction of diffusivities

The turbulent diffusivity is defined as the (negative) eddy flux of a variable, a, divided by its gradient:

$$K_a = -\frac{\overline{w'a'}}{\partial \bar{a}/\partial z}, \tag{1}$$

where z is height above ground, w vertical windspeed, the overbar indicates a temporal mean and the prime the deviation from the mean. Under stationary and horizontally homogeneous conditions, it follows from Monin–Obukhov similarity theory that

$$K_a = k u_* z/\varphi_a(z/L), \tag{2}$$

where k is the von-Kármán constant, u_* friction velocity, L the Obukhov length, and φ_a the similarity function of a (Dyer–Businger function). In the framework of MOST the φ_a for all scalar variables are equal (Hill, 1989). We require the actual shape of the similarity function only for stable conditions ($0 \leq z/L \leq 1$), which we quote from Kaimal and Finnigan (1994) as

$$\varphi_a(z/L) = 1 + 5z/L. \tag{3}$$

2.2. DIFFUSIVITIES OF HEAT AND WATER VAPOUR

We deal here with the two scalar variables temperature, T, and (specific) humidity, q, thus $a = T$ or $a = q$. The fluxes associated with these two variables are usually expressed in energy units, which gives the sensible heat flux, H, and the latent heat flux, λE:

$$H = \rho c_p \overline{w'T'}, \tag{4}$$

$$\lambda E = \rho \lambda \overline{w'q'}, \tag{5}$$

where ρ is the density of air, c_p the specific heat at constant pressure of air, and λ the latent heat of vaporization of water. The ratio of these fluxes is the Bowen ratio, or more precisely the flux Bowen ratio, β_f:

$$\beta_f = H/\lambda E, \tag{6}$$

as opposed to the gradient Bowen ratio, β_g, which is formed from the gradients using the same proportionality factors to achieve equal dimensions in numerator and denominator:

$$\beta_g = \frac{c_p \, \partial \bar{T}/\partial z}{\lambda \, \partial \bar{q}/\partial z}. \tag{7}$$

From Equations (1), (6) and (7) it follows immediately that the ratio of the diffusivities for temperature and humidity can be expressed as:

$$\frac{K_T}{K_q} = \frac{\beta_f}{\beta_g}, \tag{8}$$

so the diffusivities are equal if the flux and gradient Bowen ratios are equal. This situation is described by MOST. In situations that do not fulfil the MOST requirements of homogeneous and steady conditions, the diffusivities of temperature and humidity (or diffusivities of heat and water vapour, as they are more commonly named) need not be equal. The next two subsections describe two different mechanisms that may cause inequality of diffusivities.

2.3. INEQUALITY OF DIFFUSIVITIES DUE TO INCOMPLETE ADJUSTMENT

Consider a dry-to-wet transition with heat flux inversion over the downwind area, and treat the temperature and humidity at the upwind and the downwind area as different, distinguishable variables, e.g., T^{up} for upwind temperature and T^{dn} for downwind temperature. The diffusivity of temperature upwind of the transition is K^{up}, and that of humidity is undefined if the surface is perfectly dry. The diffusivity downwind is K^{dn}, in steady conditions identical for T^{dn} and q^{dn}, because these

two variables are perfectly correlated at their sources, which are the plant surfaces downwind of the transition. ML98 show in their Appendix A that by algebraic transformations it follows that the apparent diffusivities for the sums of the upwind and downwind variables, which are the measurable quantities T and q, obey the equation

$$\frac{K_T}{K_q} = \frac{1 + \dfrac{K^{up}}{K^{dn}} \left(\dfrac{\partial \bar{T}^{up}/\partial z}{\partial \bar{T}^{dn}/\partial z} \right)}{1 + \left(\dfrac{\partial \bar{T}^{up}/\partial z}{\partial \bar{T}^{dn}/\partial z} \right)}. \tag{9}$$

The terms in brackets are negative since we consider a situation where the temperature gradients upwind and downwind have opposite signs. With the argument that larger eddies transport the upwind scalars more effectively than the downwind scalars it can be expected that $K^{up} > K^{dn}$. From this it follows that $K_T/K_q < 1$. (This result holds true even if there is a nonzero but small upwind humidity gradient, and it is not required that the upwind diffusivity of humidity is equal to that of temperature.)

Thus, incomplete adjustment within an advective inversion downwind of a dry-to-wet transition would cause the diffusivity ratio K_T/K_q to be less than one. The ratio would be smallest near the transition and increase with increasing fetch-to-height ratio, approaching the MOST prediction of one at large fetch and close to the ground.

2.4. Inequality of Diffusivities due to Unsteadiness

ML98 propose that temporal, rather than spatial, variations of the surface conditions can cause unequal diffusivities of heat and water vapour. They call the underlying mechanism ‘unsteadiness’ because it relies on the variability of the horizontal windspeed on a time scale of several minutes, and because the surface Bowen ratio is observed to vary with time within runs of 20 min duration. An alternative way of describing the situation would be to say that the surface layer is ‘disturbed’ from above by larger-scale motions. Whatever term is used, the situation is characterized by substantial variance of the horizontal wind at low frequencies without additional net transfer of momentum. That is, the ratio of the standard deviation of windspeed to friction velocity, σ_u/u_*, is significantly larger than the consensus value of about 2.4 for the neutral limit where MOST applies (Garratt, 1992). A tidy definition of unsteadiness would require some sort of spectral filtering, but for present purposes we use σ_u/u_* as an approximate measure of the degree of unsteadiness.

In short, ML98 argue that unsteadiness of the horizontal wind causes variations of the saturation deficit near the surface, because the windspeed variations change the shape of scalar profiles in the surface layer. The evaporation rate then responds

to the changing saturation deficit near the ground. The response is such that evaporation is largest at times of highest windspeeds. This means that there exists a positive correlation between windspeed and short-term latent heat flux. The short-term sensible heat flux varies in a complementary way to the latent heat flux, constrained by the surface boundary condition of constant available energy, and is thus anticorrelated to windspeed. ML98 assume that MOST applies continuously near the ground. However, taking the mean flux over the whole averaging period, and dividing it by the gradient averaged over the same period to obtain the diffusivity defined in Equation (1), results in averaged diffusivities that are different for temperature and humidity. The reader is referred to ML98 for details. The qualitative result is that the diffusivity ratio K_T/K_q exceeds one if $\beta_g < 0$. Its exact value depends on the decoupling coefficient introduced by McNaughton and Jarvis (1983) and on a series of short-averaged statistical moments of windspeed and saturation deficit. All of these are difficult to determine accurately from experimental data.

Thus, ML98 predict that variations of the saturation deficit correlated to variations of the horizontal wind would lead, in an advective inversion, to a diffusivity ratio K_T/K_q larger than one. Because this effect would compete with the previously described effect of incomplete adjustment, it should be most noticeable well downwind of the field transition, in other words, at the base of the inversion, sometimes called the 'internal adjusted layer'.

3. Field Studies and Numerical Model of Advective Inversion

3.1. EXPERIMENTAL STUDIES

The diffusivities of heat and water vapour have been investigated in a number of studies of advective inversions downwind of a dry-to-wet transition in surface cover. The results of these studies were somewhat contradictory. Verma et al. (1978) found the diffusivity ratio, K_T/K_q, to be considerably larger than one, sometimes exceeding two. On the other hand, Lang et al. (1983) found K_T/K_q consistently less than one, often about 0.7. More recently, analysing an experiment at La Crau (France), Bink (1996) found $K_T/K_q < 1$ on average, but very sensitive to the ratio of the height of measurement to the height of the internal boundary layer (IBL). While Verma et al. (1978) and Lang et al. (1983) both operated in 'strong' advective conditions, the dataset analysed by Bink (1996) contained cases of 'strong' and 'weak' advection, where 'strong' indicates downward sensible heat flux, and 'weak' means that the sensible heat flux is reduced but still upwards. The 'weak' cases were particularly prone to scatter in the K_T/K_q values (evidently, depending on measurement height, K_T may be erratic downstream, for at each horizontal distance from the transition the vertical heat flux changes sign at some particular height). When discussing the results from our own experiment, below, we will reconsider the findings of these previous studies.

3.2. THE RWCB MODEL

Bink (1996) compared his experimental data with model predictions. For this purpose, he employed a second-order closure model introduced by Rao et al. (1974), which simulates a step change in surface conditions. Here we call it the RWCB model (initials of original and recent authors).

Bink (1996) found his implementation of the model to agree well, in general, with his experimental data, and in particular to predict $K_T/K_q < 1$ in strong advection. Although he discussed a number of limitations of the model and pointed out that 'many more cases should be studied and that general conclusions can not be drawn', he still interpreted his findings as confirming that the RWCB model was appropriate to describe the fluid dynamics in his experimental situation. He then postulated that not only in his experiment, but also those of Lang et al. (1983) and Verma et al. (1978), incomplete adjustment of the fluxes in the IBL to the abrupt change in the source-sink distributions for heat and water vapour should have caused the ratio K_T/K_q to be less than one.

To explain why Verma et al. (1978) found $K_T/K_q > 1$ instead, Bink (1996) noted that they did not measure the diffusivity ratio given by (8), but instead the ratio of the surface Bowen ratio (evaporation from a lysimeter) to the gradient Bowen ratio. While this fact may well explain some inaccuracy in their results, it does not explain why this ratio was found to exceed one as largely as it did, in apparent contradiction to the results of the other two experiments. The unsteadiness effect predicted by ML98 may be the correct explanation, but this cannot be proven in retrospect. Instrumental error is also possible.

The RWCB model has been verified to simulate advective situations well, in particular their flux-profile and flux-variance relations for temperature and humidity (Bink, 1996). In the limit $z/x \to 0$ (where x is the streamwise horizontal coordinate), MOST relationships are enforced; there is no allowance for unsteadiness. Thus, the model simulates the two-dimensional effect of incomplete adjustment as described in Section 2.3, but it ignores the correlation of the downwind saturation deficit to the unsteadiness of the horizontal wind (the 'disturbed one-dimensional' situation described in Section 2.4). By comparing our experimental data with predictions from the RWCB model, we can therefore hope to distinguish between the two counteracting effects.

3.3. OUR IMPLEMENTATION OF THE RWCB MODEL

We have implemented exactly the same set of transport equations as Bink (1996), see his Appendix A1, and used Patankar's (1980) control volume method (SIMPLE) for numerical solution. In the Results section, we compare our experimental data to simulations obtained with this implementation of RWCB.

Using the same choices of closure constants and boundary conditions as prescribed by Bink (1996), our model code essentially reproduced his simulations of his 'Run 42'. This test being satisfactory, we have adapted the boundary conditions

for the inflow and at the surface to our experimental situation. Our control volume is a rectangular domain (-20 m $\leq x \leq$ 500 m and $0 \leq z \leq$ 150 m). The step change in surface conditions is located at $x = 0$; along the top of the model domain, all properties are held constant. Model fields are iteratively refined until they meet two criteria: the largest fractional change in saturation deficit since the last cycle is required to be less than 10^{-4}, and the net flux of thermodynamic energy across the rectangular domain boundary, which should ideally vanish since this is a steady state model, is required to be no greater than 1% of the total *surface* input of thermodynamic energy, i.e. of the alongwind integral of the total surface flux $H + \lambda E$.

4. Site and Experimental

This section provides the technical description of the experiment. More details are presented than in previous publications (ML98, Laubach and McNaughton, 1998) because they will be needed frequently in the extensive quality discussion (Section 5). The subsections deal with the features of the site, the eddy correlation system to measure fluxes, the reversing system to measure gradients of temperature and humidity, the ancillary measurements required to characterize the boundary conditions, and finally the handling of the various data channels.

4.1. Site description

Our experiment was carried out over a flood-irrigated rice field at Warrawidgee, at the western border of the Murrumbidgee Irrigation Area in NSW, Australia. The site coordinates are 34°15′ S, 145°45′ E. As sketched in Figure 1, the field was of rectangular shape, orientated almost north-south (deviation $-4°$). The instruments were mounted on a steel tower of triangular cross-section, positioned close to the centre of the eastern field border to maximize fetch for westerly winds. Distances measured from the tower to the field borders were: 418 m to the west, 307 m to the north, 23 m to the east, and 271 m to the south. The adjacent land to the west was almost ideally homogeneous (flat and dry, extending for hundreds of kilometres), while in other directions there lay a patchwork of similar-sized fields with a mixture of rice, wheat, stubble and burnt stubble. Therefore, only periods with westerly winds are analysed, see Section 5.3 for details. Data acquisition equipment was placed in a caravan parked on the driveway east of the field.

The field itself was laser-levelled. Above the mineral soil there was a layer of 0.03 m loose material (soil and organic), and above that a water layer of 0.17 m. During the experiment, the height of the rice crop grew from 0.77 m to 0.86 m, relative to firm ground, and the canopy density also increased. While initially there were a few small patches of open water visible from the top of the tower, most of them were filled and covered by the rice crop at the end of the experiment.

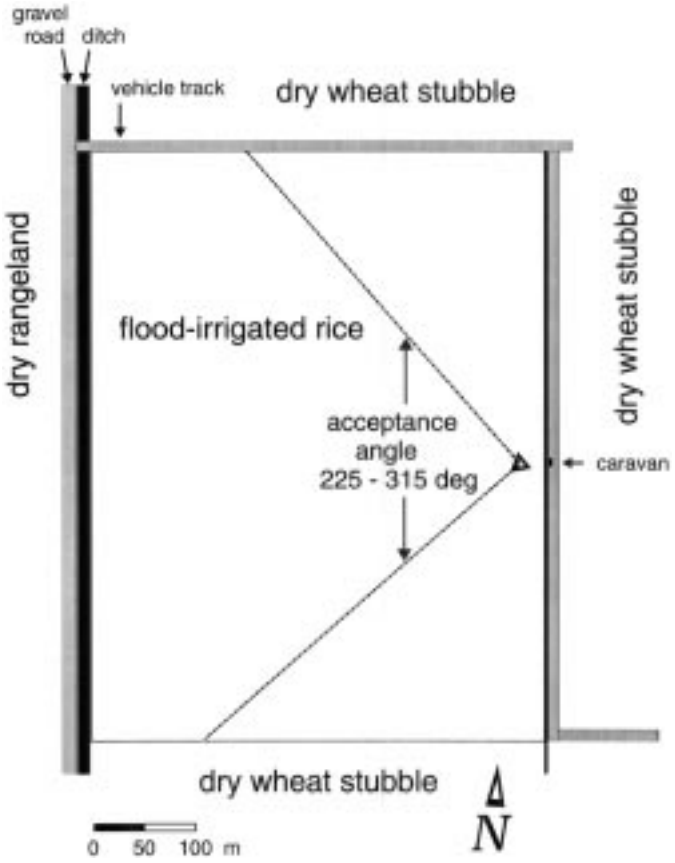

Figure 1. Plan of the measurement site at Warrawidgee. The position of the tower is indicated by a triangle (size exaggerated), the range of accepted wind directions by dashed lines.

4.2. FLUX INSTRUMENTATION

Fluxes of sensible heat, latent heat, and carbon dioxide were measured at two heights, with identical eddy correlation systems. (The carbon dioxide fluxes are not presented in this paper.) The heights were 2.0 m and 3.9 m, respectively, above the zero plane displacement, which was estimated as two-thirds of the canopy height above water level (Oke, 1987). For winds from NW to SW these heights corresponded to fetch-to-height ratios from 100:1 to 150:1 at the upper level and twice these values at the lower level. Referencing the measurement heights against the water surface gives 2.4 and 4.3 m, while the canopy height of the rice relative to the water surface is 0.6 to 0.7 m. Accordingly, our measurements were above the roughness sublayer if we follow Kaimal and Finnigan (1994) in assuming that this sublayer extends to about three canopy heights.

Each eddy correlation system consisted of a 3-dimensional sonic anemometer, Model CSAT-3 (Campbell Scientific, Logan, Utah), an open-path infra-red gas ana-

lyzer (IRGA) for water vapour and carbon dioxide similar to the one described by Auble and Meyers (1992), and a fast-response chromel-constantan thermocouple (Type E) of diameter 12.7 μm (1/2000″). The sonic probe was mounted on the western side of the tower and the IRGA 0.3 m south-east of the sonic path. The thermocouple was placed besides the centre of the IRGA path, 0.05 m away, and at a horizontal distance of 0.25 m from the sonic path. The thermocouple was used for two reasons. First, it avoided the need to correct sonic temperature fluctuations for humidity fluctuations (Schotanus et al., 1983), which would have been significant at the Bowen ratios occurring in our experiment (typically -0.1 to -0.8). Second, placing the thermocouple close to the humidity sensor ensured that flux losses due to spatial separation from the wind sensor were of similar magnitude for temperature and humidity fluxes. This was advantageous since the ratio of the two fluxes was of particular interest.

4.3. GRADIENT INSTRUMENTATION

Vertical gradients of temperature and humidity were determined at the same two heights as the fluxes. The gradients were approximated from the finite differences, ΔT and Δq, between air drawn from 0.30 m above and 0.30 m below each height. Each set of temperature and humidity differences was obtained from a pair of Humitter 50Y sensors (Vaisala, Helsinki, Finland). These sensors use a capacitance measurement for relative humidity and a platinum-film resistance measurement for temperature. Specific humidity can then be calculated from relative humidity and temperature. Each Vaisala sensor was placed inside a white-painted double shield and ventilated at a rate of approximately 4 m s^{-1}. We replaced the original membrane filters protecting the sensors with fine nylon gauze in order to reduce the response time.

To remove calibration offsets between the two sensors forming a pair, their positions were interchanged during each averaging period. This was achieved using a reversing system designed similarly to that of Bland et al. (1996), driven by a step motor. Action of the motor was triggered by the data acquisition computer, in phase with the completion of averaging periods. Two full reversing cycles were carried out during each period. The ‘switch time’, i.e., the time while the system was reversing, was excluded from the calculation of the gradients, as was an additional time span after reaching the new position, in order to allow the sensors to adjust fully to the new temperature and humidity values. We will refer to the sum of the switch time and the adjustment time as ‘dead time’, and discuss its impact on measurement precision further below.

4.4. ANCILLARY INSTRUMENTATION

This subsection describes other instruments on the site. Data from these are needed to specify input parameters for the advection model.

A number of sensors were installed in order to determine the energy available for turbulent heat fluxes. A net radiometer CN-1 (Middleton Instruments, Melbourne, Australia) mounted at 6.8 m above water level provided measurements of the radiative input. Two flux plates gave estimates of the soil heat flux, and were placed under the loose material on the firm ground, one of them beneath a dense part of the rice canopy, the other beneath a less dense part. Finally, heat storage in the water layer, expected to be a significant term in the energy budget, was determined using two sensors providing depth-integrated averages of the water temperature, placed close to the flux plates. Each water thermometer was made of a series of thermocouple junctions in a 215-mm long non-transparent plastic tube. The tube was then fixed to the ground by a nail and stood almost vertically in the water by means of its own buoyancy.

We also measured conditions within the rice canopy. We operated a Vaisala Humitter 50 Y sensor (also with the membrane filter replaced by a lighter gauze) near the estimated displacement height of the crop. The intake height was set initially to 0.36 m above water level, and was raised twice during the experiment to adjust to the growing crop. The final height was 0.46 m above water level. This sensor was placed 5 m north-west of the tower. We obtained measurements of radiative surface temperature from an infra-red thermometer, model KT-15 (Heitronics, Wiesbaden, Germany). This was mounted on the tower, at 6.7 m above water level at a viewing angle of 45° from nadir, facing south-west. From the instrument's characteristics it follows that it viewed an area of about 0.45 m in diameter at the crop surface.

4.5. Data collection

All data collection was handled by a single desktop computer, thus ensuring automatic synchronization of flux and gradient measurements. Eddy correlation data were sampled at 10 Hz, gradient data and ancillary data at 1 Hz; averaging periods were 20 minutes long. The gradient systems were reversed every five minutes to obtain two full cycles in each averaging period.

Sonic anemometer data were transferred to the computer via serial ports, which meant they retained their maximum resolution of 19 bits. IRGA data were sampled by a 16-bit A/D plug-in board (National Instruments, Austin, Texas). Thermocouple voltages were measured by a datalogger CS-21X (Campbell Scientific, Logan, Utah), which provided an internal temperature reference and temperature-shielded connectors. The data were, however, not stored by the datalogger. Instead, they were converted to amplified, linearized analog output signals, which were then read into the computer via the 16-bit A/D board. This way of using a 21X as a thermocouple amplifier avoided the problem of transferring small voltages over long distances.

The gradient and ancillary sensors all operated with voltage outputs. These were sampled by a multiplexing extension of the 16-bit A/D board.

5. Data Analysis

The purpose of this section is to assess rigorously the quality of our data, which is crucial for later conclusions. The first two subsections discuss errors and corrections of the eddy flux data and of the gradient data, respectively. The last subsection gives the criteria we used to accept or reject data runs, and defines two quality classes that will be used in Section 6.

5.1. FLUX ERRORS

Our main aim is to assess the diffusivity ratio K_T/K_q. To minimize its error it is necessary to minimize the errors of the flux Bowen ratio, β_f, and the gradient Bowen ratio, β_g. We deal first with the flux Bowen ratio, noting that we do not need to discuss the accuracy of the wind fluctuations, because their error affects H and λE equally. Besides, the generally high quality of the CSAT-3 sonic anemometer has been shown in a number of comparison experiments, e.g., Foken et al. (1997), Vogt et al. (1997). Also, we do not need to discuss the flux losses due to horizontal displacement of the temperature and humidity sensors from the wind sensor in this context, because we matched these losses for H and λE closely by placing the thermocouple next to the IRGA. We did, in fact, correct the fluxes for this separation error following a procedure described elsewhere (Laubach and McNaughton, 1998), but this correction does not alter the flux Bowen ratio. Errors that might affect the flux Bowen ratio are those that are specific to either the temperature or the humidity sensors. Therefore, we have to address the calibrations and the response times of these sensors.

Measuring temperature fluctuations with a thermocouple has virtually no calibration error, because the relation of the voltage to the temperature difference depends only on which species of metals are joined, and is almost linear. Errors in the reference temperature ('cold junction') affect only the mean, not the fluctuations. The two remaining possible sources of systematic errors are: the response time of the sensor due to its thermal inertia, and radiative heating. It is shown in Appendix A, below Equation (A3), that for our 12.7 μm thermocouple the time constant is 0.0043 s at a windspeed of 4 m s^{-1}, which causes negligible flux loss. It is also shown there (Table AI) that the heat flux error due to radiation is about 3 W m^{-2} at cloud-free solar noon conditions, and less otherwise. Since the radiation error always feigns an apparent upward heat flux, while H is consistently downward in our experiment, this effect results in a systematic underestimation of $|H|$, but by 1% or less.

Humidity measurement with the IRGA entails three possible sources of error: the instrument's calibration, the underestimation of high-frequency fluctuations due to path averaging, and the error due to density variations. The IRGAs were calibrated before and after the experiment, and on two occasions during the field campaign run side-by-side for a few hours to check for disagreements. No drift

in their sensitivity for absolute humidity was found. To assess the significance of path averaging, we used the transfer functions as given by Moore (1986). It was found that, in the presence of separation flux losses as mentioned above, the path averaging of the IRGA causes an underestimation of λE by about 2% at 2.0 m height, and half as much at 3.9 m. Since the effect was so small, no correction was applied. Finally, the flux error due to density effects was removed following Webb et al. (1980); the 'Webb correction' was small but systematic – it reduced λE by between 0.3 and 6.5%, as β_f ranged from -0.10 to -0.83.

Combining these errors of the thermocouple and IRGA measurements, we find that the flux Bowen ratio is likely to be overestimated by 1% on average, after corrections as described. On individual runs, a statistical sampling error of a few percent can be expected in addition to that.

While minimizing the error of the flux Bowen ratio is crucial to obtain reliable diffusivity ratios, we note that we also require small absolute errors of H and λE for the purpose of estimating K_T and K_q separately and comparing them with MOST predictions and numerical simulations. With corrections as described above, we obtained good closure of the surface energy budget (Laubach and McNaughton, 1998). This is an indication that absolute errors of the fluxes were small and not systematic.

5.2. GRADIENT ERRORS

The turbulent diffusivity of a scalar variable a (e.g., temperature or humidity) is calculated from the ratio of the flux and the vertical gradient of a, as given in Equation (1). An error in K_a can arise from an error in either the measured flux or the measured gradient, unless the relative errors of both are identical. The latter is possible if the 'fast' a sensor (used to determine the flux) and the 'slow' a sensor (used to determine the gradient) are subject to a consistent but wrong calibration. In other words, absolute calibrations are not needed to give accurate values of K_T and K_q; instead, internal consistency of the field calibrations of the T and q sensors is sufficient.

Our temperature data from Warrawidgee show sufficient consistency without any correction procedure (Figure 2). The 'slow' data in this figure are obtained by averaging the temperatures from the two sensors of the reversing pair. We find a clear linear relationship, with the slope of 'fast' versus 'slow' sensors to be 1.008 at both measurement heights, i.e., the difference in systematic calibration errors is below 1%. We also find an offset in these plots, but that affects neither the flux nor the gradient measurement.

For humidity, a two-step correction procedure was required to achieve consistency. These corrections were carried out with the original relative humidity (RH) values, before computing specific humidity. The first step was removal of a small linear drift with time, possibly caused by contamination of the sensor. The second correction was found to be necessary after calibration checks in the laboratory,

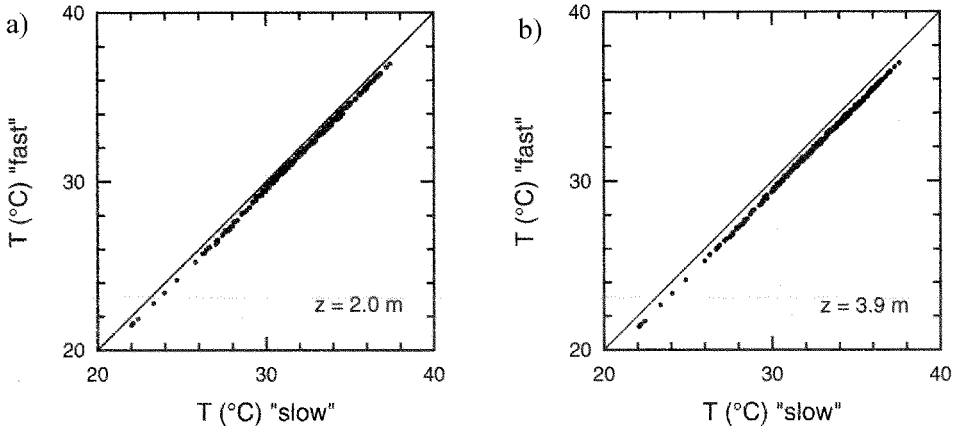

Figure 2. 20-minute-averages of temperature from eddy correlation ('fast') versus gradient system ('slow') (a) at 2.0 m above displacement height, (b) at 3.9 m. Also drawn is the 1 : 1 line for comparison. Slopes of linear regression are 1.008 in (a) and (b). Displayed data cover the whole experimental period.

using a dewpoint generator to provide air of known humidity. These checks revealed that the manufacturer's linear formula that converted output voltage to RH did not account for a change of sensitivity somewhere in the range between 30 and 40% RH, a range that was not uncommon in our experiment. To correct for the inappropriate linearization, we matched the 'slow' RH data with the 'fast' data separately for three ranges: below 25% RH and above 56% RH, linear fits were used, and in the intermediate range a 5th-order polynomial was fitted, with the boundary conditions of continuity and continuous derivative at the joints with the linear regions. The fitting procedure was carried out for each pair in a reversing system, not for individual sensors.

The success of these calibration corrections can be assessed in Figure 3, showing specific humidity from the eddy correlation sensor (IRGA) versus specific humidity calculated from the Vaisala sensors. The relationships are found to be linear and constant with time. The slope of linear regression is 0.998 at 3.9 m and 1.007 at 2.0 m. Combined with the results for the temperature sensors, we conclude that calibration errors of the gradient instrumentation do not bias the diffusivity ratio K_T/K_q by more than 1%.

There are, however, some other characteristics of the gradient systems' design that can introduce errors to the gradient Bowen ratio, β_g. These error sources are associated with the response times of the sensors, the 'dead time' of the reversing cycle, and the relations between these times.

The first issue in this context affects the humidity measurement only. The Vaisala sensor measures relative humidity directly, and the temperature signal must be used to convert this to either absolute or specific humidity. For highest precision, it is thus desirable to match the response times for the temperature and humidity

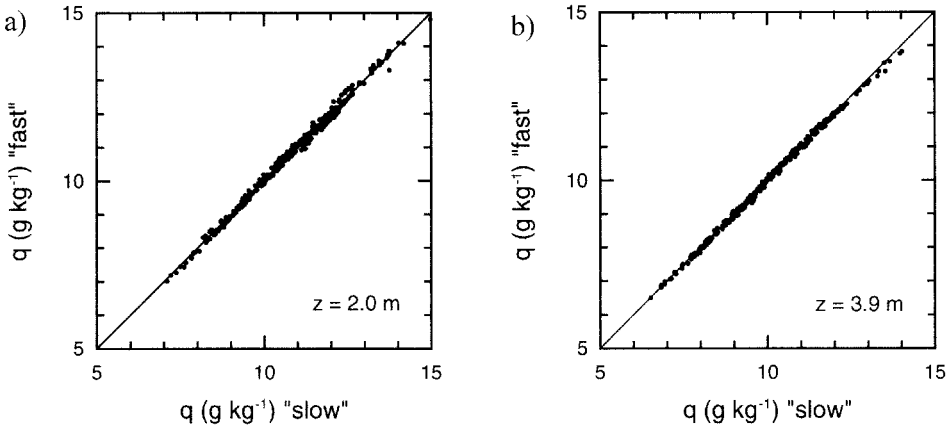

Figure 3. Same as Figure 2, but for specific humidity, after corrections as described in the text. Slopes of linear regression are 1.007 in (a) and 0.998 in (b).

sensor before computing the humidity conversion. Neglecting this will not have any visible effect on the 20-minute averages of q as shown in Figure 3, and so overall consistency of the q calibration is not compromised. A mismatch of time constants may, however, introduce additional scatter on the determination of Δq. To determine the time constants, a few time series collected at Warrawidgee were investigated. The data from the slow sensors were compared to those from the fast sensors, with the latter block-averaged to simulate reference time series sampled at 1 Hz. For humidity, the data of the 'slow' sensors matched the reference closely, indicating that the response time of the Vaisala humidity sensors was less than 1 s. For temperature, it was found that the platinum films in the Vaisalas were considerably slower. Close match was achieved when applying a recursive digital filter with a time constant of 16 s to the temperature reference. Consequently, in all further processing the 'slow' relative humidity data were subjected to this recursive filter in order to achieve matching response times in the gradient data.

The response times have to be known for a second reason: in order to choose an appropriate dead time to allow adjustment of the sensors to their new sampling height after reversing their positions. If the dead time is too short, adjustment will be incomplete and the gradient will be underestimated. This is unimportant if the response times of temperature and humidity sensors are closely matched. If they are not, then a short dead time will introduce a systematic bias of $\Delta T/\Delta q$ and, consequently, β_g. One might thus be tempted to allow for a long dead time to prevent such a bias. There is, however, a penalty for an excessively long dead time, in that it reduces the time fraction of valid gradient samples within the averaging period. In principle, fluxes and gradients should be measured over identical averaging periods. In practice, because of the need for a dead time in the reversing cycle, there will be a sampling mismatch: the fluxes are calculated from 100% of the samples within the averaging period, while the gradients are calculated from the subperiods

between the dead times only. In order to keep the sampling mismatch small, the time fraction of these valid subperiods should be made as long as possible. This requirement is in conflict with the need to allow slow sensors to adjust to their new positions.

To resolve this conflict, response times of the humidity and temperature sensors were matched as described above, and the dead time varied to see if it influenced the results for β_g. Dead times of 20, 40, and 60 s were tried, and for each dead time β_g at 3.9 m was plotted versus β_g at 2.0 m, as well as β_g versus β_f at either height. It was found that regression results for these types of plots varied very little, and certainly not systematically with dead time. The correlation coefficients with 40 s were slightly higher than with 20 s and not less than with 60 s, so that 40 s appears to be the best possible choice of dead time. On the one hand, this value is 2.5 times the estimated time constant of the platinum films, implying that the sensors have adjusted to 91.6% of the step change due to reversing. (Clearly, without previously matching the humidity data to the platinum films' time constant, $|\Delta T/\Delta q|$ would be severely underestimated.) On the other hand, allowing 40 s dead time for each of the four reversals within a 20-min period results in a time fraction of valid data of 86.7%. This ensures a reasonably good match with the flux sampling.

The procedures described above ensure as far as possible that there is no bias in the gradient Bowen ratio, and that its statistical sampling error is not significantly larger than that of the flux Bowen ratio. Unfortunately, we had an unexpected noise problem in our analog data acquisition, with frequent electronic spikes in our recordings. This had no effect on the flux measurements, since the wind data were recorded digitally, and thus any noise in the fast temperature and humidity data was uncorrelated to the w fluctuations and did not impact on the calculated covariances. The noise did, however, hamper the accuracy with which small gradients could be detected. After a few days of data had already been collected, we managed to reduce the occurrence of spikes significantly by careful investigation for desired and undesired earth connections in the entire experimental setup. We do not dismiss the earlier data entirely, but we assign them to a 'Class 2', which we consider to be less reliable than 'Class 1', see below for details. We were able to restore high quality in the temperature data by a software routine for automatic spike elimination; however this was less successful for the humidity data because of a higher signal-to-noise ratio.

Finally, we estimate the resolution of ΔT and Δq, by investigating the offsets that are removed by the reversing procedure. If such offsets were constant in time, then we should not see any variability. The variability present in practice reflects statistical or time-dependent errors, either of instrumental nature (true resolution of the sensors and the data acquisition) or due to sampling uncertainties (true meteorological differences between the subperiods sampled in the different sensor positions). For temperature, we found that the variability of the removed offset decreased with increasing ΔT, indicating that small gradients are uncertain because of true sampling variability, and that its standard deviation was 0.026 K. This value

is assumed to reflect the random error of ΔT. For humidity, the variability did not decrease with Δq, because of the noise problem mentioned above, and the standard deviation of the removed offset was 0.045 g kg^{-1}. We take this value as the statistical error of Δq.

5.3. DATA SELECTION

The experiment ran from January 19 to February 9, 1997. Measurements were taken during daylight hours, with about 300 runs recorded; all of these are shown in Figures 2 and 3. The number of runs is reduced in the following by applying a number of quality criteria, the most important being fetch. We reject a run if the mean wind direction lay outside the western quarter (225 to 315°), as indicated in Figure 1. This is equivalent to demanding that the mean fetch over the period exceeded 405 m, which is more than 100 times the upper measurement height and 200 times the lower height. We also demand that the instantaneous wind direction be within the western bisector (180 to 360°) for at least 99% of the time, to exclude transition periods and excursions from the eastern field border. This leaves a total of 46 runs at either height. With only four exceptions each, they all represent stable conditions with z/L in the range 0.009 to 0.4. The exceptions are four periods of higher stability (z/L taken at 2.0 m). In these, the time series of humidity at 3.9 m showed subperiods of virtually no variance, while the short-term mean reached a well-defined minimum. This indicates incursions of unmodified air from above the IBL down to 3.9 m. These incursions did not reach the 2.0 m level. Because of this, the 20-min averages of the heat fluxes at 3.9 m were about 20% less than at 2.0 m. Without going into a detailed discussion we note that the observed behaviour can be interpreted as a combination of advection and disturbance. Suffice to say here that we dismiss these four runs because conditions were obviously nowhere near those of a constant-flux layer. However, the results we present in Section 6.3 below seem to indicate that, in general, we did not encounter the problem of insufficient fetch.

We split the 42 remaining periods into two classes by applying two more criteria. ‘Class 1’ are our best data, ‘Class 2’ we consider to be less reliable. Data are assigned to Class 1 only if they were collected after January 25, which was the day when we succeeded in reducing electronic noise, and if ΔT exceeded 0.08 K, which is three times the resolution of the gradient system as estimated above. (Applying an analogous criterion for humidity would not exclude any of the points meeting the first two criteria.) Following this selection, Class 1 comprises 24 runs at 2.0 m and 22 runs at 3.9 m.

6. Results and Discussion

In the first part of this section, the meteorological situations represented by the selected 42 runs are described. In the following subsections, these runs are analysed

with the ultimate aim of verifying the prediction of ML98 about the non-equality of the diffusivities of temperature and humidity in a disturbed surface layer. Since our experiment was carried out at the base of an advective inversion, it may be that the effects of unsteadiness, whose existence we set out to prove, are confounded with those of advection. We must therefore show that the latter were minor, which we do in three steps. First we assess how well the normalized standard deviations of the wind components and scalars conform to MOST predictions. Second, we show that the flux divergences between the two measurement levels were small, and that they are correctly simulated by the numerical advection model. Third, we demonstrate that the gradient Bowen ratio did not depend on height. After these required preliminaries, we compare the measured diffusivities against both MOST predictions and numerical model simulations (Section 6.5), we show that the average diffusivity ratio K_T/K_q agrees with the prediction of ML98 (Section 6.6), and finally we search for parameters determining the actual value of K_T/K_q.

6.1. METEOROLOGICAL SITUATION

The synoptical situation over Australia in January 1997 was unusual, and resulted in generally light to moderate winds at Warrawidgee, frequently from the northeast and therefore unfavourable for our experiment. There were two favourable exceptions from this main pattern: westerlies occurred from late afternoon of January 21 until the evening of the 22nd, before winds turned south and on the next day a cold front passed through; and westerlies also persisted from February 7 to 9. Otherwise, acceptable wind directions were spread over several short periods in between, none of them longer than four consecutive runs. On January 26, several local thunderstorms occurred, some with heavy rainfall. However, the rangeland dried out completely over the next few days, while we did not record a single run of acceptable wind direction. Daytime temperatures (at 3.9 m) were 27 to 34 °C, specific humidities 8 to 14 g kg^{-1}.

It is the result of this overall meteorological situation that only 42 runs fulfilled the selection criteria as described above. Each of them represented, more or less, one of the following situations (distinctions are not strict because characteristics of the three groups overlap somewhat):

– Light to moderate winds (2 to 5 m s^{-1}), cloud-free mornings and variable but little cumulus cloud cover in the afternoons, convective upwind conditions. Downwind available energy exceeded 400 W m^{-2}, downwind Bowen ratio ranged from -0.1 to -0.3, and the 'unsteadiness parameter' σ_u/u_* was typically found between 3.4 and 5.0.
– Moderate winds (3 to 5 m s^{-1}), fairly steady (σ_u/u_* from 2.8 to 3.7), and heavily overcast skies. This resulted in downwind available energy less than 400 W m^{-2} and downwind Bowen ratios of -0.4 to -0.8. This situation persisted during the last three days, February 7 to 9.

– Moderate southwest winds (5 to 8 m s^{-1}), again fairly steady (σ_u/u_* from 2.6 to 3.5), but little cloud cover. Downwind Bowen ratios were then typically -0.3 to -0.4. Most, but not all, of these runs occurred on 22 January, before we managed to reduce noise levels in the gradient data, and were thus allocated to Class 2. As a consequence, average stability of Class 2 was less than that of Class 1.

Having thus characterized the meteorological conditions, we are able to specify the input parameters for the numerical simulation of the advective inversion. We do this in Appendix B.

6.2. NORMALIZED STANDARD DEVIATIONS OF WIND AND SCALARS

The first step of the data analysis aims to assess how closely our measurements resemble those taken in a horizontally homogeneous surface layer, where MOST applies. MOST predicts that the standard deviations of the wind components, normalized by friction velocity, approach constant values in the neutral limit. According to Garratt (1992), these values, as found from numerous experiments, are about 2.4 for σ_u/u_*, 1.9 for σ_v/u_*, and 1.25 for σ_w/u_*. In stable conditions, similar or slightly higher values are typical. It has also been found experimentally that the standard deviations of scalar variables, normalized by their respective surface scales ($T_* = |\overline{w'T'}|/u_*$ for temperature and $q_* = |\overline{w'q'}|/u_*$ for humidity) approach a constant value somewhere near 2 (de Bruin et al., 1993). In Figure 4, we investigate these predictions for the five variables mentioned, by plotting the standard deviation of each against the corresponding scaling parameter. The values for u_*, T_*, q_* are taken at 2.0 m, assuming that they approximate the surface values closely enough. (Evidence that this assumption is valid is given in the next subsection.)

In the first panel of Figure 4, it is shown that the vertical wind fluctuations closely obey MOST, at both measurement heights. This is an important indication that our fetch-to-height ratio is large enough that momentum transport is in equilibrium with the local surface. Finding the MOST relationship for σ_w/u_* valid does not only indicate horizontal homogeneity, it also helps to justify the usage of σ_u/u_* as an unsteadiness parameter. It can be seen in the next two panels that the standard deviations of the horizontal wind components, σ_u and σ_v, exceed the MOST values considerably and consistently, indicating strong and frequent unsteadiness. In other words, there are significant wind fluctuations present that are not associated with momentum transport. This is a clear signature of what is sometimes called ‘inactive motion’ (e.g., Katul et al., 1996), though we avoid this expression here because we will see below that the role of these wind fluctuations in scalar transport seems to be an ‘active’ one. Values for σ_u/u_* range from 2.6 to 5.0, for σ_v/u_* from 2.2 to 5.8. Those at 3.9 m are greater than those at 2.0 m. For both levels, they are on average higher than those reported from the La Crau experiment, where σ_u/u_* over the dry upwind plain was closer to 2 than to 3 in the majority of runs (de Bruin et al. 1993, their Figure 9).

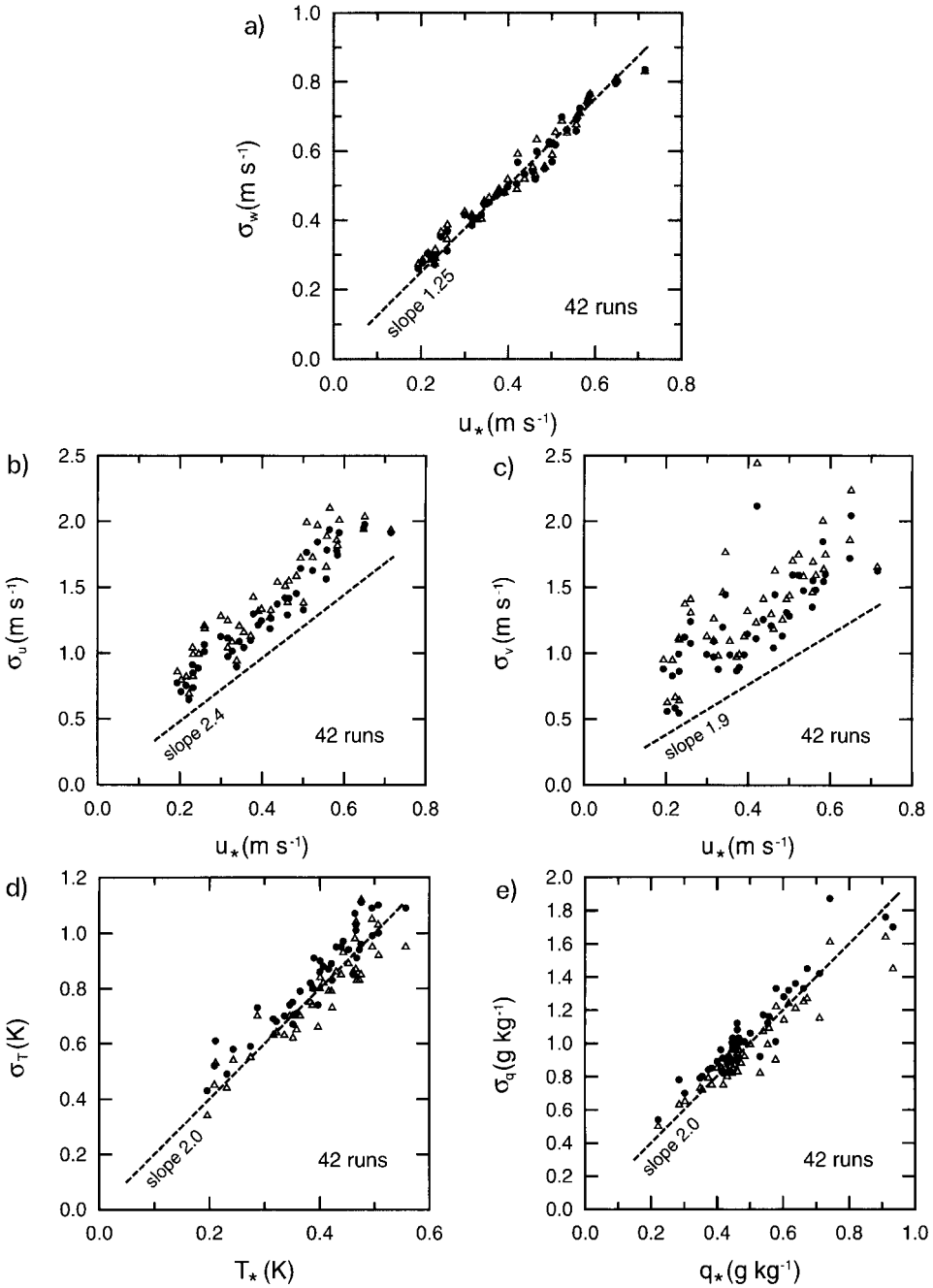

Figure 4. Standard deviations for (a) vertical wind, (b) longitudinal wind, (c) lateral wind, (d) temperature, (e) specific humidity against their corresponding surface scales. Dots: 2.0 m, triangles: 3.9 m. Shown as dashed lines are the values expected for horizontally homogeneous conditions and in the limit of neutral stratification (slopes as indicated, zero offsets).

In the last two panels of Figure 4, the standard deviations of T and q are shown. The overall behaviour of the two scalars is similar: most, but not all, points are found slightly above the dashed line indicating the neutral limit of MOST. The range covered by the data is well within the ranges reported from other experiments. Thus, in general scalar fluctuations are not very different from those in a homogeneous surface layer. Closer inspection reveals that the standard deviations at 3.9 m tend to be a little less than those at 2.0 m. This trend is more noticeable for humidity than for temperature, and may indicate some influence of the upwind surface on the data at 3.9 m. Since the upwind surface is dry, humidity fluctuations vanish there. If unmodified, or only partly modified, upwind air reaches the sensor during some fraction of the averaging period, then the resulting humidity variance for the whole period will be less than for air that is fully in equilibrium with the evaporating crop. This can happen either when the IBL is shallower than the measurement height, indicating advection, or alternatively when large eddies subside from the convective boundary layer aloft, displacing the IBL temporarily. Subsiding air would show little temperature fluctuations, too, in agreement with the slight trend in Figure 4d.

6.3. FLUX DIVERGENCE

In this subsection we assess the flux divergences, which are attributed to inadequate fetch (local advection). This is done by symmetrical linear regression of the fluxes at 3.9 m against those at 2.0 m. ('Symmetrical' means that the distances of the data points from the fitted line, whose sum is minimized by the regression, are taken perpendicular to the regression line, and not, as usually, perpendicular to the abscissa.) For all three variables shown in Figure 5, that is, for friction velocity, sensible heat flux, and latent heat flux, there is good correlation between heights. The obtained slopes are 1.02 for u_*, and values a little below one for the scalar fluxes: 0.88 for H and 0.93 for λE, respectively. The deviation of the slope from one is a direct measure of flux divergence. The fact that we find little flux divergence between levels means that the fluxes measured at the lower height closely represent the surface fluxes from the rice field. In other words, most of the time the 2.0-m level is in the well-adjusted layer at the base of the advective inversion, where conditions should deviate little from Monin–Obukhov similarity theory (MOST). This situation is consistent with the assumptions made in the theoretical paper by ML98.

Having shown that a one-dimensional description using MOST provides a valid first-order approximation of several features of our experimental situation, we turn our attention to the RWCB model, which should describe the deviations due to small advective effects. In Figure 6 it can be seen that the model runs (with input parameters as specified in Appendix B) simulate the flux divergences correctly. The measured and modelled ratios of the flux at 3.9 m to that at 2.0 m are presented, both for sensible and latent heat. They are plotted against stability for two reasons: first, to show how well the model runs cover the range of stability found in the

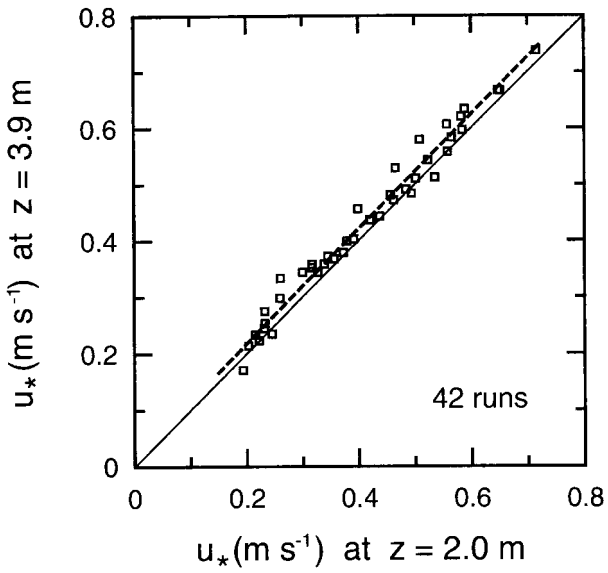

Figure 5a. Friction velocity at 3.9 m versus friction velocity at 2.0 m. Symmetrical linear regression (dashed line): slope 1.018, offset 0.014 m s^{-1}, squared correlation coefficient 0.98.

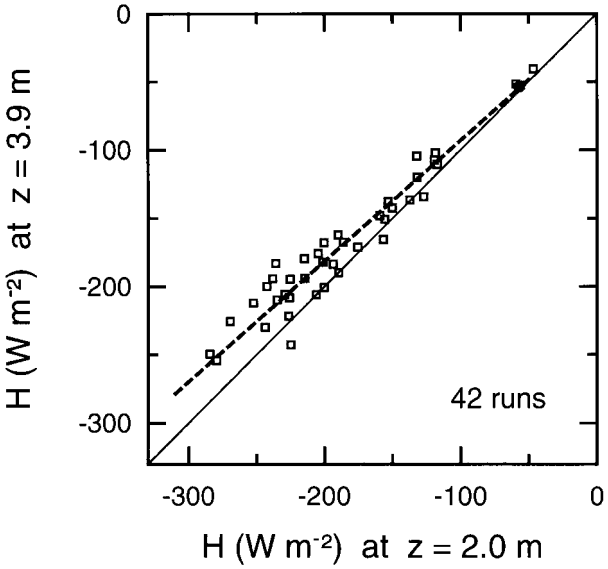

Figure 5b. Sensible heat flux at 3.9 m versus sensible heat flux at 2.0 m. Symmetrical linear regression (dashed line): slope 0.88, offset -4.7 W m^{-2}, squared correlation coefficient 0.94.

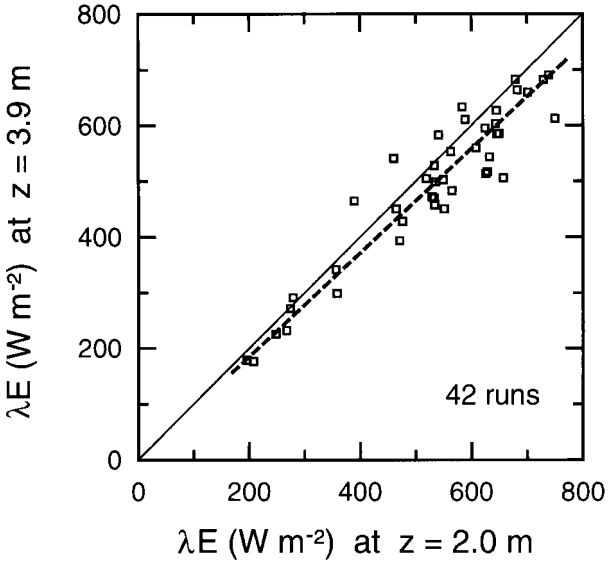

Figure 5c. Latent heat flux at 3.9 m versus latent heat flux at 2.0 m. Symmetrical linear regression (dashed line): slope 0.93, offset -1.7 W m^{-2}, squared correlation coefficient 0.89.

experimental data, and second, to show that there is no simple relationship between flux divergence and stability, neither in the modelled steady conditions nor in the field data. If there was a relation, then it would be because stability affected the height of the IBL. However, we do not find such a relation because, both in model and experiment, the IBL properties respond to several parameters, of which friction velocity and the absolute size of the step change in available energy are the most variable.

Not only does the model give the right magnitude of the flux ratios (range 0.82 to 0.96, with most points near the centre of the cloud of experimental data), it also predicts correctly that when approaching neutral stratification the sensible heat flux varies more strongly with height than the latent heat flux. This is not a numerical effect due to small flux values: we obtained the smallest z/L not when H was small, but when u_* was large, in both model and experiment. Because of that, the data points appearing as 'near-neutral' typically represent the *largest* downward sensible heat fluxes, of order -200 W m^{-2}. The finding that in these runs the divergence of H depends more strongly on stability than that of λE reflects that the magnitude of the step change is different for T and q, and that the two-dimensional dynamics of the advective situation enforce different flux-profile shapes for these two scalars. One could say that at highest windspeeds the advection of sensible heat is largest. For latent heat, on the other hand, flux divergence varies little with stability.

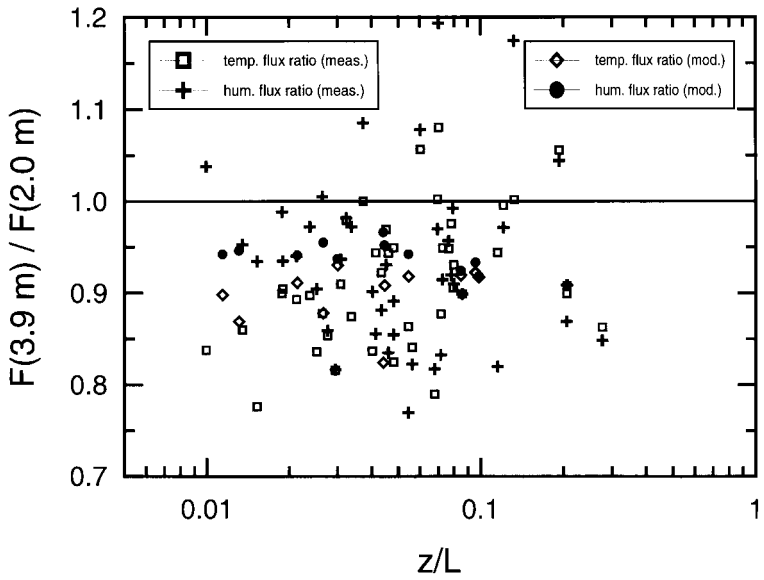

Figure 6. Ratio of the flux at 3.9 m to the flux at 2.0 m, for sensible heat and latent heat, versus stability parameter at 2.0 m. Experimental data are: squares for H, crosses for λE. Also shown are those 11 runs of the RWCB model that produced numerically stable results: diamonds for H, dots for λE. Model fluxes are taken at 447 m downwind of the step change in surface properties.

6.4. HEIGHT VARIATION OF GRADIENT BOWEN RATIO

In the surface layer, the gradients of temperature and humidity vary strongly with height. We find their values at 3.9 m to be typically about half of those at 2.0 m. However the ratio of temperature and humidity gradients, which is proportional to the gradient Bowen ratio as defined by (7), should be approximately constant with height. Figure 7 shows that this is indeed the case at Warrawidgee: linear regression yields a slope of 0.97. This finding is consistent with the results of the RWCB advection model (shown as dots): the modelled gradient Bowen ratios differ never by more than 4% between heights. It is also consistent with results of Lang et al. (1983) in a very similar experimental situation, in their Figure 4, the gradient Bowen ratios from three heights (1.13, 1.81 and 4.54 m above water level) are shown to be in close agreement with each other.

Finding such small height dependence of the gradient Bowen ratio, for our own experiment as well as that of Lang et al. (1983), indicates that the horizontal distance between measurement location and field border was in both experiments large enough that the gradients of T and q were in local equilibrium with the evaporating surface up to at least 3.9 m.

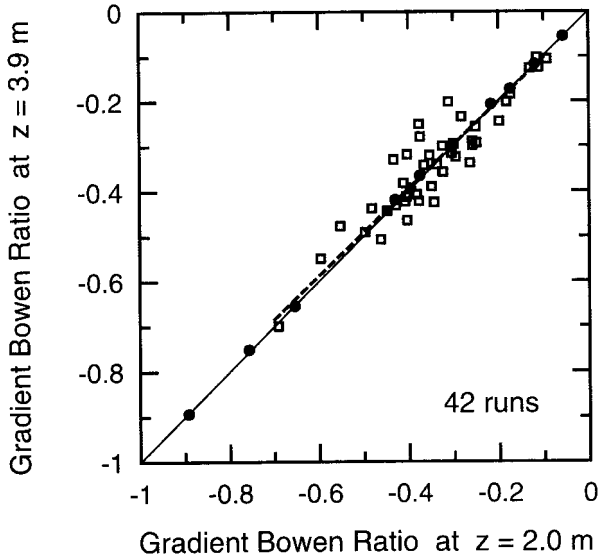

Figure 7. Gradient Bowen ratio at 3.9 m versus gradient Bowen ratio at 2.0 m. Experimental data are shown as squares, symmetrical linear regression of them as a dashed line: slope 0.97, offset −0.0077, squared correlation coefficient 0.85. Also shown are the 11 runs of the RWCB model (dots).

6.5. DIFFUSIVITIES AS MEASURED, MODELLED, AND PREDICTED FROM MOST

We turn now to the main objective of this analysis, the investigation of the diffusivities for heat and water vapour. They were calculated according to their definition (1), both for our 42 experimental runs and the 11 valid runs of the RWCB model. Alternatively, the diffusivity for any scalar can be predicted from MOST, i.e., by applying (2). The results of these calculations are presented in Figure 8 for heat and in Figure 9 for water vapour.

First we discuss the results at 2.0 m height, shown in the left-hand panel of either figure. The overall picture is much the same for heat and water vapour. The most remarkable observation is that both MOST and RWCB values underestimate the experimental values, typically by about 20%. We return to this later in this subsection. We observe further that, at 2.0 m height, the RWCB model runs predict very similar diffusivities to those in a homogeneous surface layer, as given by MOST, with one exception. The exception is the run with the lowest windspeed, where the RWCB values exceed the MOST value considerably. In this run the ratio of the sensible heat fluxes, as shown in Figure 6, is as low as 0.82, indicating incomplete adjustment of the flow to the downwind surface. This means that at low windspeed advection works to increase the diffusivity, according to the model. However, the close agreement of RWCB and MOST results in all other model runs indicates that for a large range of conditions advection had a minor influence on our measurements at 2.0 m.

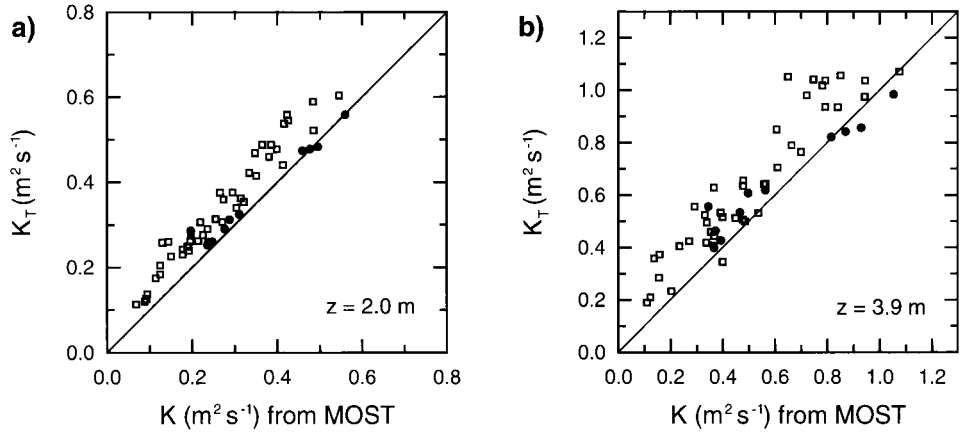

Figure 8. Diffusivity of heat from 42 experimental runs (squares) and from 11 RWCB model runs (dots), each calculated as the ratio of flux to gradient given in Equation (1), versus diffusivity predicted from Monin–Obukhov similarity theory (MOST) given in Equation (2), (a) at 2.0 m above displacement height, (b) at 3.9 m.

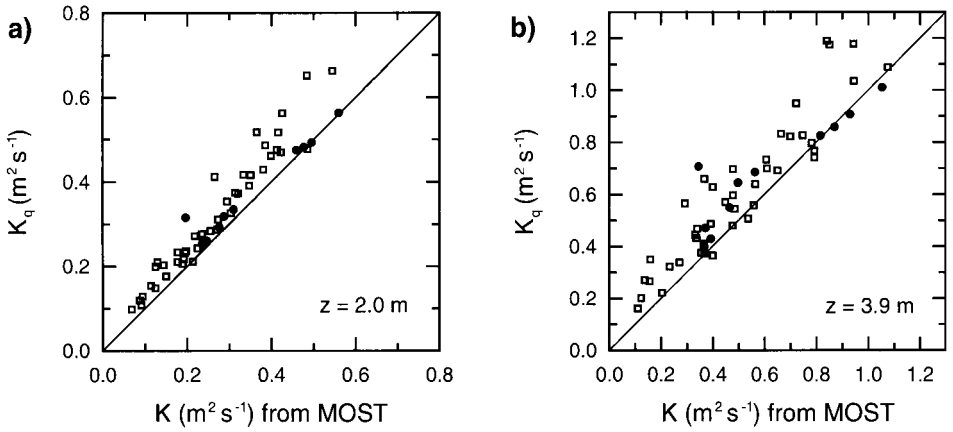

Figure 9. Same as Figure 8, but for diffusivity of water vapour.

The picture is somewhat more complicated at 3.9 m height, shown in the right-hand panels of Figure 8 and Figure 9. For low to moderate diffusivity values (corresponding to low to moderate windspeeds) the RWCB model predicts higher diffusivities than does MOST. The opposite is true for the largest three values, at high windspeeds, although the differences there are small. That is, the RWCB model predicts that advection will have a noticeable effect on eddy diffusivities at 3.9 m for lower windspeeds. In addition, we note that, as at 2.0 m, the RWCB simulations underpredict the measured scalar diffusivities, with the same single exception. The difference between model and experiment is obvious in all four panels, but most noticeable for the diffusivity of temperature at higher windspeeds.

These results show that the scalar diffusivities in our experiment are larger than can be accounted for by advection alone. This is particularly so at 2.0 m where the RWCB model predicts that advection should have very little effect on scalar diffusivities. The enhanced diffusivity values do, however, support our interpretation of the cospectra of vertical wind and scalar variables obtained from the Warrawidgee data. These show enhanced flux at low frequencies, and we associate this with interaction between the surface layer and the larger-scale motions overhead (McNaughton and Laubach, 2000).

It might be argued that, alternatively, scalar diffusivities are expected to be enhanced when measured in the roughness sublayer close to the canopy top (Kaimal and Finnigan, 1994). These authors give three times the canopy height (referenced to ground, not displacement height) as the approximate upper limit of this sublayer. We measured higher than that, so we do not expect roughness effects to be the main cause for enhanced diffusivities. Also, if the enhancement was due to roughness sublayer behaviour, it should decrease with height. Instead, it is at least as noticeable at 3.9 m as it is at 2.0 m, supporting our interpretation that unsteadiness is the main cause.

6.6. AVERAGE OF THE DIFFUSIVITY RATIO

Having analysed the diffusivities separately, we now investigate their ratio, K_T/K_q. According to MOST, it should be exactly one. In 10 of the 11 valid RWCB model runs, we find it in the range 0.97 to 1.00 at z = 2.0 m (average 0.99), and 0.90 to 1.00 at z = 3.9 m (average 0.97). For the exceptional case at low windspeed, the diffusivity ratio is 0.91 at 2.0 m and 0.79 at 3.9 m. In being less than or equal to one, these numbers agree with Equation (9). They indicate that not always, but for a wide range of conditions, the advective situation causes little deviation from MOST at the upper level, and virtually none at the lower. It is therefore sufficient to compare the experimental values for K_T/K_q to the MOST value of one in the following.

In Figure 10, the diffusivity ratio is shown against the local stability parameter, z/L. Full symbols represent runs from Class 1 and open symbols represent runs from Class 2, as defined in Section 5.3. We choose stability as the abscissa variable, not because a relationship is expected, but because this allows comparison with similar figures in the literature (Verma et al., 1978; Lang et al., 1983). As can be seen, the experimental values of the ratio are somewhat scattered but most are greater than one. Table I presents this result statistically, by giving the mean diffusivity ratios for different subsets of our data. The table also gives standard deviations for these subsets, indicating considerable scatter. We note that the scatter for the Class 2 subset at 3.9 m is twice as large as for both Class 1 subsets. It is likely that this is due to the electronic noise in the gradient data. The scatter of the Class 1 data is about 10%, which is the magnitude expected from instrument accuracies and sampling statistics. For Class 1 from both heights, the average K_T/K_q = 1.10,

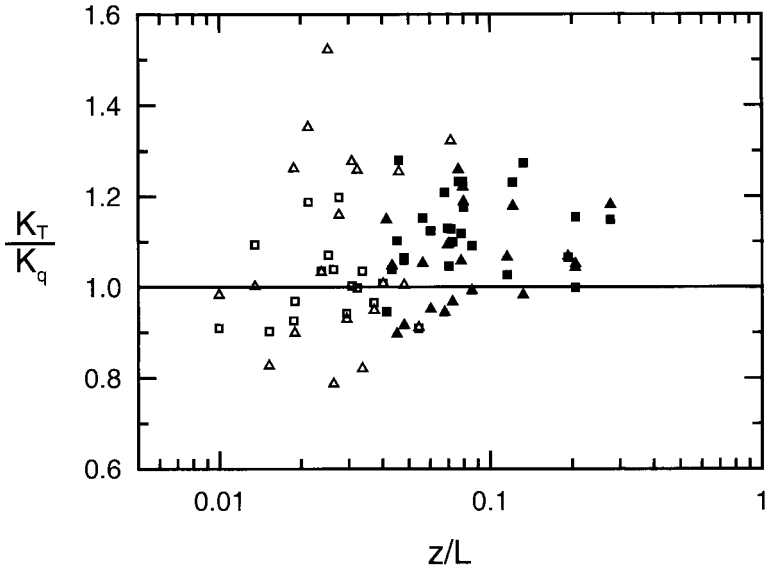

Figure 10. Diffusivity ratio K_T/K_q versus stability parameter. Squares: 2.0 m, triangles: 3.9 m. Full symbols stand for runs from Class 1 (best data), open symbols for runs from Class 2, as defined in Section 5.3.

TABLE I

Average diffusivity ratio, K_T/K_q, for various subsets of the experiment at Warrawidgee. The given uncertainties are standard deviations of the samples, and the numbers in brackets are sample sizes.

z (m)	Class 1 only	Class 2 only	Class 1 and Class 2
2.0	1.13 ± 0.09 (24)	1.01 ± 0.09 (18)	1.08 ± 0.10 (42)
3.9	1.06 ± 0.10 (22)	1.08 ± 0.21 (20)	1.07 ± 0.16 (42)
2.0 and 3.9	1.10 ± 0.10 (46)	1.05 ± 0.16 (38)	1.07 ± 0.13 (84)

with a standard deviation of 0.10. Thus, the average value is one standard deviation larger than exact unity, which would be the value expected from MOST. Assuming normal distribution of the scatter, which seems reasonable from Figure 10, one can interpret this result statistically, by saying that the probability of K_T/K_q being more than one is 0.84. If we repeat the same calculation for the Class 1 data at 2.0 m only, because close to the ground the gradients are larger and thus known more accurately than higher up, we find that the average (1.13) exceeds one by 1.4 times the standard deviation of the sample (0.09), resulting in a probability of 0.92 for $K_T/K_q > 1$.

As Figure 10 shows, the Class 2 subsets represent atmospheric conditions closer to neutrality than the Class 1 subsets. This is because Class 2 includes the majority

of data obtained at higher windspeeds. Most of the runs with high windspeed happened to occur on January 22, before we succeeded in reducing noise levels. The rest of them did not satisfy the condition of $\Delta T > 0.08$ K, which is not surprising because small gradients are most likely to occur at high windspeeds. Some of these runs show $K_T/K_q < 1$, which may be due to incomplete adjustment (since conditions of high windspeed and large downward heat flux are highly advective). However, other runs in this class show extremely high diffusivity ratios, which illustrates the level of uncertainty and justifies our judgment that the data quality of these runs is poorer than that of Class 1. If the Class 2 data are included to assess the statistics of K_T/K_q, then the scatter increases, the average at 2.0 m moves close to the average at 3.9 m, but the average at 3.9 m does not change significantly. This gives us confidence that the result of $K_T/K_q > 1$ still holds for slightly stable conditions.

Finding the diffusivity ratio to be larger than one is in agreement with our theoretical predictions due to the effect of unsteady winds and associated fluctuations in surface saturation deficit and surface fluxes (ML98). It is also in qualitative agreement with the experimental results of Verma et al. (1978), but disagrees, though, with the results of Lang et al. (1983), and those of Bink (1996) analysing the La Crau experiment. In these two studies, diffusivity ratios less than one were found. The disagreement of our data with those from La Crau can be understood from the finding that our flux data show little height divergence, as demonstrated above. At La Crau, flux divergences were much larger (cf. Bink, 1996; Chapter 5.2). Bink also found the La Crau data to be described well by the advection model of RWCB. This means that at La Crau the main mechanism causing deviations from transport similarity for T and q was incomplete adjustment of the IBL to the new underlying surface. At Warrawidgee this was not the case.

More difficult to explain is the disagreement with Lang et al. (1983), because our measurement situation was very similar to theirs. They obtained diffusivity ratios K_T/K_q from 0.61 to 1.01, with the smallest values at the largest stabilities, while we found 1.10 on average, and no dependence on stability (Figure 10). Lang et al. discussed in detail some possible atmospheric mechanisms to explain their results, but mentioned measurement errors only briefly. We examined their likely errors as far as possible in retrospect. Doing so, we found a high likelihood that Lang et al. underestimated the flux Bowen ratio, β_f, systematically, and consequently underestimated K_T/K_q. The main reason for this is the slow response of the thermocouple used in their eddy correlation system. Details are presented in Appendix A. Unfortunately, the predicted loss of heat flux depends critically on the exact thickness of the thermocouple wires, which is somewhat uncertain. We therefore cautiously suggest that Lang et al. (1983) may have encountered true diffusivity ratios much closer to one than the published values. This would reduce the disagreement with the K_T/K_q values at Warrawidgee by a considerable degree. All other experimental results of Lang et al. (1983), including spectral shapes, are very similar to ours.

In summary then, we have found the theoretical prediction of ML98, that K_T should exceed K_q by about 10% in the conditions at Warrawidgee, to agree with the direct experimental result that $K_T/K_q = 1.10$. No doubt such excellent agreement is fortuitous, but it is clear that a K_T/K_q ratio greater than one could not have been caused by advection. Our experiment therefore gives strong support for the proposal that unsteadiness of the surface fluxes can lead to dissimilarity in averaged diffusivities.

6.7. Dependence of the diffusivity ratio on other variables

An interesting question is: can the observed spread of the diffusivity ratios be attributed to some functional dependence on other variables? Figure 10 demonstrates no relationship with stability; further, our data indicate no dependence of K_T/K_q on wind direction or available energy. Another possibility could be non-stationarity of boundary conditions. We tested if K_T/K_q was related to the variation coefficient (standard deviation divided by the average) of net radiation, with negative result. For all these variables, including stability, the squared correlation coefficient is less than 0.1.

There appears to be a dependence on windspeed, as shown in Figure 11: K_T/K_q decreases with increasing $\bar{u}$. The trend is noteworthy, but inconclusive with regard to whether advection or unsteadiness determines the diffusivity ratio. Values of K_T/K_q less than one appear mainly at high windspeeds, which may indicate some influence of advection in those runs. However, as shown in Section 2.3 and by the results of the RWCB model, advection can never explain a K_T/K_q value in excess of one. Such values we find frequently at low windspeed. When mean windspeed is low, then unsteady winds, due to convective structures in the planetary boundary layer overhead, are most likely to have a significant effect. Thus, unsteadiness seems to provide the correct interpretation of at least the left half of Figure 11.

To test the relative contributions of advection and unsteadiness, we require suitable parameters characterizing the two mechanisms. The best parameters available to quantify advection are, in absence of any upwind measurements, the divergences of sensible and latent heat flux. The diffusivity ratio does not correlate with either of them (squared correlation coefficient less than 0.05), which reconfirms the earlier conclusion that advection had only a minor effect on the vertical transport of scalars in our experiment.

As explained in Section 2.4, the parameter σ_u/u_* provides some measure of unsteadiness. In Figure 12, we test whether the diffusivity ratio K_T/K_q depends on this parameter. As noted earlier, the σ_u/u_* values spread well above the steady limit of 2.4, which is indicated in the figure. At 2.0 m we find a weak positive correlation (squared correlation coefficient 0.19), and at 3.9 m, a positive correlation is found only with the Class 1 data, not with Class 2. The slope for the Class 1 data at 3.9 m is the same as for the data at 2.0 m. Thus, linear regression results suggest that the diffusivity ratio tends to increase with σ_u/u_*. This is some, though admittedly

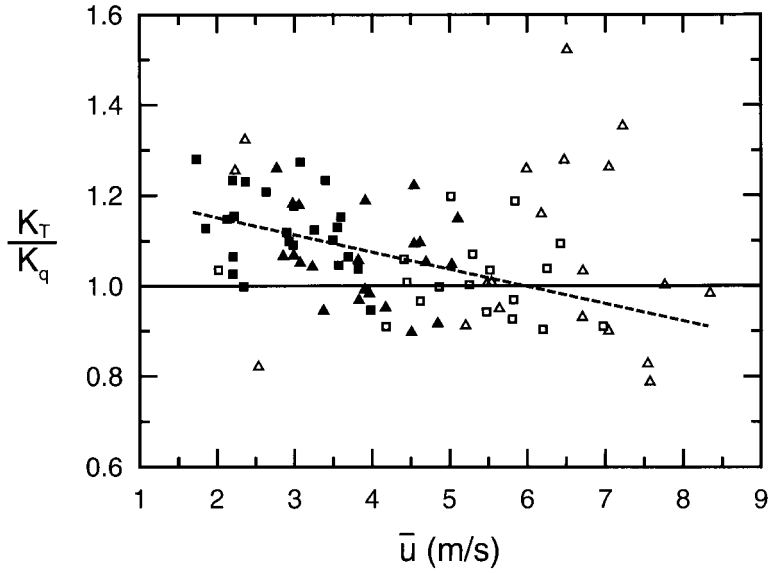

Figure 11. Diffusivity ratio K_T/K_q versus mean horizontal wind. Symbols are as in Figure 10. The dashed regression line is valid for 2.0 m (slope −0.038, offset 1.23, squared correlation coefficient 0.30, 42 points).

weak, indication that unsteadiness is the main mechanism causing $K_T/K_q > 1$. We do not claim that the relationship between K_T/K_q and σ_u/u_* has to be linear, the regression line in Figure 12 is intended to be illustrative rather than definitive.

7. Summary and Conclusions

The results of this paper support the contention that eddy diffusivities for scalars in a disturbed, but otherwise uniform surface layer do not obey Monin–Obukhov similarity theory. They also support the contention that two separate mechanisms cause this departure from ideal behaviour. The first is that disturbance of the surface layer increases the 'eddy diffusivity' of every scalar by creating additional flux at low frequencies. This flux contribution is not associated with the local scalar gradient. The exact mechanism driving it is uncertain, but it probably involves substantial updrafts and downdrafts interacting with the surface layer, these being associated with shifts in wind strength and direction aloft. The spectral evidence for this enhancement of scalar fluxes is given elsewhere (McNaughton and Laubach, 2000).

The second mechanism is that variations in windspeed driven by larger-scale processes above the surface layer cause changes in momentum transfer from one brief period to another, and that this causes scalar concentration gradients and hence scalar fluxes to vary in step with the changes in windspeed. This effect is

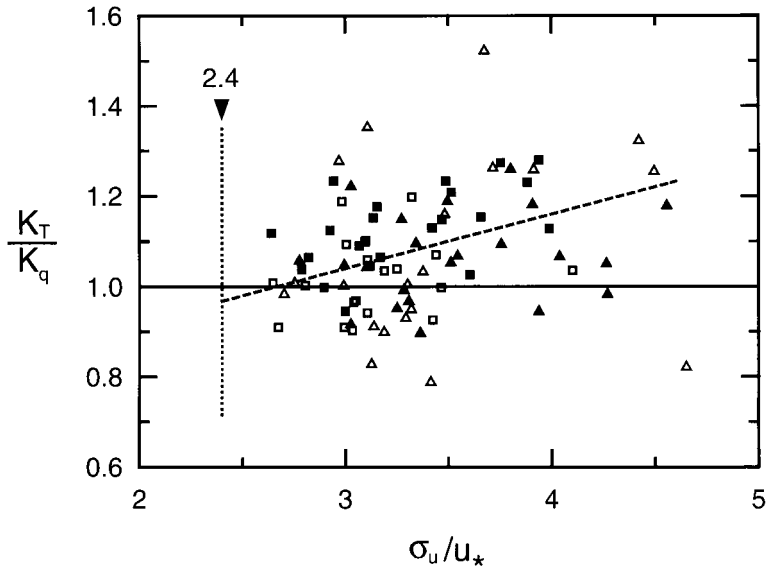

Figure 12. Diffusivity ratio K_T/K_q versus unsteadiness parameter of horizontal wind, σ_u/u_*. Symbols are as in Figure 10. The dotted vertical line at 2.4 indicates the limit of ideal Monin–Obukhov similarity theory. The dashed regression line is valid for 2.0 m (slope 0.12, offset 0.68, squared correlation coefficient 0.19, 42 points).

greater for scalars whose release is sensitive to surface concentration, and less for scalars that are not so sensitive. The result is that relationships between mean fluxes and mean gradients over a typical measurement period (order of magnitude of 10^3 s) encompass a range of conditions. In this situation, eddy diffusivities do not average linearly. In particular, the theory developed in ML98 predicts that K_T/K_q should exceed one in an unsteady stable surface layer over a freely transpiring crop. The data we obtained at Warrawidgee indicate a diffusivity ratio of 1.10 on average, strongly supporting the theoretical predictions of ML98.

The competing mechanism of advection, i.e., incomplete adjustment of the fluxes downwind of a step change in surface conditions, would result in $K_T/K_q < 1$. In our experiment this was observed only in a minority of runs because our measurement positions were far enough downwind and low enough to render advection minor. The opposite situation seems to have been the case in the La Crau experiment analysed by Bink (1996). The diffusivity ratio there tended to be less than one, and the fact that flux divergences were larger than at Warrawidgee supports Bink's conclusion that incomplete adjustment was the reason for this.

Our result of $K_T/K_q > 1$ agrees qualitatively with that of Verma et al. (1978). This may mean that their experiment was, similar to ours, carried out far enough downwind of the field transition to make unsteadiness the main mechanism affecting the diffusivity ratio. However, care is required not to overinterpret their results, because their experimental errors using the lysimeter technique were probably

larger than the errors in the more recent experiments using the eddy correlation technique.

Our result disagrees substantially with that of Lang et al. (1983), who found K_T/K_q typically near 0.7. Because their range of Bowen ratios as well as their fetch-to-height ratio were similar to ours, it is unlikely that incomplete adjustment of the fluxes to the downwind surface was important in their experiment, but not in ours. Instead, based on careful error estimates, we suspect that instrumental errors might have biased the results of Lang et al. towards significant underestimation of K_T/K_q. This interpretation is supported by finding that the results of the two experiments were very similar in many other respects, including height constancy of the gradient Bowen ratio and shapes of the cospectra of temperature and humidity fluxes.

Bink (1996) interpreted the diffusivity ratios reported by Lang et al. (1983) as being in qualitative agreement with the RWCB advection model. However, a closer look reveals that K_T/K_q values as low as 0.7 are not simulated by the model for their experimental conditions (which resembled ours at 2.0 m height very closely). Our model runs representing such conditions, i.e., cloudless and with windspeeds of 4 to 6 m s^{-1}, give 0.97 to 0.98 for the diffusivity ratio at 2.0 m (0.90 to 0.94 at 3.9 m height). The values of Lang et al. are about 20 to 35% less. Were they correct, they would not be fully compatible with the RWCB model. This incompatibility is resolved if instrumental errors played a larger role than the mechanism of incomplete adjustment in producing the results of Lang et al. (1983).

We could not deduce from our data further details of how the diffusivity ratio at the base of the IBL depends on other parameters of the atmospheric surface layer. This failure is due to the error spans encountered in this type of experiment, and there is not much hope to reduce them significantly with current techniques. The only additional, but not very certain, result is a tendency of K_T/K_q to increase with the normalized standard deviation of windspeed, σ_u/u_*, which may be considered as an unsteadiness parameter.

From a purely practical perspective, it may be sufficient to conclude that the diffusivity ratio at the base of an advective inversion is not very far from one, so that gradient techniques may safely be employed in order to derive fluxes with little additional error. However, from a theoretical perspective our results are important, since they show that unsteadiness of the horizontal wind (or, more precisely, the disturbances caused by such unsteadiness) can enhance scalar diffusivities substantially. The presence of unsteadiness can also be detected in the shapes of the cospectra of scalar fluxes and the power spectra of wind and scalars (McNaughton and Laubach, 2000). To extend Monin-Obukhov similarity theory in such a way that the effects of unsteadiness are included remains a future challenge.

Acknowledgements

Our research was supported by the Marsden Fund (administered by the Royal Society of New Zealand), under contract No. CO6539. The experimental work and most of the data analysis were carried out while JL and KGM were employed by the Horticulture and Food Research Institute of New Zealand. JDW acknowledges support from the Natural Sciences and Engineering Research Council of Canada (NSERC).

We are indebted to a number of people who contributed to the success of our experiment. We thank Mark Astill for building the reversing systems and helping to prepare the various instrument mounts, and Phil Prendergast for support during the preparation phase and the field experiment. We are obliged to the colleagues of NIWA (Gracefield, NZ) and FIAMS (Adelaide) for each lending us an IRGA, and in particular to Peter Isaac for calibrating these devices. We are grateful to Peter Coppin and Ray Leuning (CSIRO Land and Water, Canberra) for providing the tower, power generator and air-conditioned caravan, and also to Greg Foster who organized the transport of these items, as well as some purchases, for us. John Blackwell and his staff of CSIRO Land and Water at Griffith provided accomodation and local services, and Angelo Silvestro allowed us to work on his ideally located paddy field.

Appendix A: Sensible Heat Flux Error Using a Thermocouple

In the body of this paper it was noted that the diffusivity ratios K_T/K_q calculated from data obtained at Griffith by Lang et al. (1983), henceforth L83, do not agree with those from Warrawidgee presented in this paper, despite the fact that experimental conditions were rather similar at the two sites. The Griffith experiment was carried out 16 years before the Warrawidgee experiment, when some procedures to correct for flux losses were not well-known. This made us re-examine the possible role of measurement errors in the interpretation of data from the Griffith experiment. Especially the heat flux errors introduced by L83's rather bulky temperature sensor were of concern. There are two such errors: one due to the sensor's response time, the other due to radiative heating. We investigate both of them, in separate sections.

1. Response time of a cylindrical temperature sensor

Thermocouples, and many other types of temperature sensors, work on the principle of exchanging heat with the medium whose temperature is to be determined, and tracking this exchange. Inherent to this principle is a characteristic response delay, dependent on properties of the medium and the sensor. In other words, the sensor acts as a low-pass filter, which can be expressed by a gain function, or

transfer function, in the frequency domain. As with Moore (1986), we assume a first-order gain function for the thermocouple response:

$$G_r(f) = [1 + (2\pi f \tau)^2]^{-1}. \tag{A1}$$

In this equation, the response time, τ, is estimated following Jacobs and McNaughton (1994). There,

$$\tau = c_m \rho_m b V (A k_a Nu)^{-1}, \tag{A2}$$

where V is the volume, A the surface, and b a typical length scale of the sensor (diameter for a cylinder), c_m the specific heat per mole and ρ_m the molar density of the sensor material, k_a the molecular thermal conductivity of still air (0.027 W m^{-1} K^{-1} at 25 °C), and Nu the Nusselt number. L83 used a copper-constantan thermocouple. For copper, c_m = 24.47 J mol^{-1} K^{-1} (at 25 °C and constant pressure), and $\rho_m = 1.40 \times 10^5$ mol m^{-3}. For other metals, both properties are less than 5% different, so that we can use these numbers for our estimate. We then assume a cylindrical shape of the thermocouple, although in the contact region of the two metals the actual shape might well be different. It should be noted that if the shape is not cylindrical because two wires are welded together, then the effective diameter will be larger than the nominal diameter of a single wire. For a cylinder, $V A^{-1} = 0.25\, b$, and

$$Nu = 0.21 + 0.57 Re^{0.5} \tag{A3}$$

where $Re = ub\nu^{-1}$ is the Reynolds number, ν being the kinematic viscosity of air (1.7×10^{-5} m^2 s^{-1}). There are different empirical fits for Nu available in the literature, e.g., from Moore (1986) and Jacobs and McNaughton (1994). We choose to follow the more recent version by Jacobs and McNaughton (their Equation 3b), but to approximate it with the exponent set to 0.5, giving (A3), because this will simplify some steps further below. With Re approaching zero, all the fits converge.

Inserting the given constants, we obtain τ as a function of u and b. Because of $Nu \sim Re^{0.5}$ the relations are approximately $\tau \sim u^{-0.5}$ and $\tau \sim b^{1.5}$. For instance, at $u = 4$ m s^{-1} the response time is τ = 0.0043 s for a thermocouple of diameter b = 12.7 μm (our experiment), τ = 0.037 s for b = 50 μm, and τ = 0.11 s for b = 100 μm.

For our experiment at Warrawidgee we can conclude that the resulting flux loss is negligible. This would still be so if the effective diameter of the thermocouple at the point of welding was twice the nominal diameter (25.4 μm), resulting in τ = 0.013 s. Flux losses in the experiment of L83 are not negligible, though. Their thermocouple was constructed from two wires, each of 50 μm in diameter; records of how the wires were joined appear to be lost. We inserted the τ values for b = 50 μm and b = 100 μm to (A1) and multiplied the resulting transfer function with two others, one representing a separation from the wind sensor of 0.05 m

and the other approximating an analog Bessel filter as used by L83. Application of the resulting total transfer function to model cospectra (Kaimal et al., 1972), for a range of windspeeds and stabilities, yielded heat flux losses of order of 20 to 45% using b = 50 μm and 30 to 60% using b = 100 μm. Proceeding similarly to assess the error of latent heat flux, caused by a sensor separation of 0.10 m and the Bessel filter, resulted in 20 to 40% flux loss. An indication that the fluxes H and λE measured by L83 were indeed subject to severe losses is found in their Figure 3, where each of the fluxes appears systematically closer to the zero line than its counterpart calculated from the gradient measurements (subscript g). In this figure, $H/H_g \approx 0.6$ ($\pm$ 0.1) and $\lambda E/\lambda E_g \approx 0.75$ ($\pm$ 0.2).

Whatever the true diameter of their thermocouple was, it seems that L83 underestimated the ratio $H/\lambda E$ systematically. For a more precise assessment it would be critical if the effective diameter equalled the nominal diameter of the single wire, which was 50 μm, or if it was larger because the two wires were welded or soldered in parallel.

2. Radiation error of sensible heat flux

We follow largely the ideas of Jacobs and McNaughton (1994), abbreviated JM94 in the following. A temperature sensor exposed to radiation is warmer than the ambient air. We define the excess temperature T_e as the temperature of the wire, T_m, minus ambient air temperature, T. T_e depends on the amount of radiation absorbed by the wire as well as its ventilation rate. Using the sensor to derive sensible heat flux, H, will be subject to an error, because instead of the fluctuations of air temperature, T', the fluctuations of sensor temperature, $T'_m = T' + T'_e$, are obtained and subsequently correlated with the vertical wind fluctuations, giving an apparent heat flux that is proportional to

$$\overline{w'T'_m} = \overline{w'T'} + \overline{w'T'_e}. \tag{A4}$$

JM94 show that the error term can be written as

$$\overline{w'T'_e} = \frac{\partial T_e}{\partial u}\,\overline{w'u'}. \tag{A5}$$

JM94 then derive this term explicitly for a flattened wire only, but provide all necessary relations to do the same for a cylinder. Undertaking this, we start by inserting JM94's Equation (2) into their Equation (4), which gives the following expression for T_e:

$$T_e = a(1+\alpha)Qb(\pi k_a)^{-1}Nu^{-1}, \tag{A6}$$

where Q is the global irradiation, α the albedo of the underlying surface, and a the absorption coefficient of the wire for shortwave radiation. JM94 found a = 0.6,

TABLE AI

Radiation error of sensible heat flux, $H_e = \rho c_p \overline{w'T_e'}$ (in W m^{-2}), obtained using temperature data from a cylindrical sensor of diameter b, for global irradiance Q = 1000 W m^{-2} and albedo α = 0.2, at different windspeeds u. Corresponding momentum fluxes are taken from our experimental data.

u (m s^{-1})	$-\overline{w'u'}$ (m^2 s^{-2})	H_e at b = 12.7 μm	H_e at b = 50 μm	H_e at b = 100 μm
2	0.04	1.1	2.7	4.2
4	0.18	2.0	4.7	7.0
8	0.72	3.1	7.0	10.3

which is the assumed value here. The u dependence of T_e is contained in the Nu dependence, hence

$$\frac{\partial T_e}{\partial u} = -\frac{a(1+\alpha)Qb}{\pi k_a Nu^2}\,\frac{\partial Nu}{\partial u}. \tag{A7}$$

Insertion of (A7) with (A3) into (A5) and some algebraic transformations lead to

$$\overline{w'T_e'} = -\frac{a(1+\alpha)Q}{2\pi k_a}\left[0.077\left(\frac{u\nu}{b^3}\right)^{1/2} + 0.42\frac{u}{b} + 0.57\left(\frac{u^3}{b\nu}\right)^{1/2}\right]^{-1}\overline{w'u'}, \tag{A8}$$

which is the desired expression for the heat flux error of a cylindrical sensor exposed to radiation and ventilation. Strictly speaking, $\overline{w'u'}$ in (A5) and (A8) is not the (kinematic) momentum flux, because in this expression u represents the magnitude of the windspeed over the sensor and not the streamwise component of the wind vector, but the difference can be neglected.

Let us abbreviate the expression within square brackets in (A8) by [...]. Inserting values for u, b, and ν as in the previous section shows that the last of the three terms in [...] dominates. Note that although [...]$^{-1}$ decreases with increasing u, the absolute error of the heat flux increases, because the momentum flux increases with u^2. In other words, we get the counter-intuitive result that the radiation error of the heat flux is largest when ventilation is strongest! To assess the importance of the radiation error, consider the numbers given in Table AI. There, a global irradiance Q = 1000 W m^{-2} and an albedo α = 0.2 have been assumed, and the error (multiplied by ρc_p to obtain energy units) is given for three windspeeds and three sensor diameters. An irradiance of the assumed magnitude occurs only on clear summer days around noon. Only then, and only for the thickest sensor, the error reaches more than a few W m^{-2} (which is still of order of 2% of net radiation only). At all other times the radiation error is even smaller. This means it can be neglected in our own data as well as in those of L83.

The sign of the radiation error is always that of an upward heat flux. Since the experimental situation considered here is a stable IBL, we deal with downward heat fluxes. Thus the error reduces the magnitude of H slightly. This, in turn, reduces the diffusivity ratio K_T/K_q. Even while we neglect the radiation error because of its small magnitude, we keep in mind that in stable stratification it can only cause a decrease of apparent K_T/K_q, never an increase.

Appendix B: Input Parameters for the RWCB Advection Model

In our experiment we did not measure upwind conditions, so we are unable to simulate individual experimental runs with the RWCB advection model. We thus limit our concerns to checking how well the general characteristics of model predictions match the observed characteristics. For this we need only ensure that the input parameters and variables used in the simulations encompass an appropriate range of meteorological conditions and crop characteristics.

TABLE BI

Input parameters for the numerical simulations (RWCB model). Friction velocity, u_*, is assumed constant across the field border. Available energy, A, is given for the downwind surface; temperature, T, and specific humidity, q, are values at 3.9 m height upwind of the border. In the last column, the stability parameter z/L (at z = 2.0 m) is given as calculated by the model, provided that the run produced a numerically stable solution.

Special conditions	u_* (m s^{-1})	A (W m^{-2})	T (°C)	q (g kg^{-1})	z/L
Windy	0.74	300	29	11	0.011
–	0.66	100	32	11	0.027
–	0.66	300	32	11	0.021
–	0.66	500	32	11	0.013
Evening	0.44	25	32	11	0.099
–	0.44	100	32	11	0.085
–	0.44	300	32	11	0.055
–	0.44	500	32	11	0.027
Dry	0.44	500	32	8	0.044
Hot, dry	0.44	300	35	8	0.096
–	0.30	100	32	11	No convergence
–	0.30	300	32	11	No convergence
–	0.30	500	32	11	0.044
Humid	0.30	500	32	14	< 0
Cool, dry	0.30	500	27	8	< 0

Inputs that the RWCB model needs to simulate the advective inversion are: the friction velocity in the approach flow, reference values of mean temperature and humidity at a single point in the flow, and both the upwind and downwind values for roughness length, available energy, and either surface resistance or latent heat flux. Of these, friction velocity, temperature, humidity and available energy are varied between model runs, as shown in Table BI, while the other parameters are assumed constant, as given below.

Let us first discuss the upwind parameters. We assume that friction velocity and roughness length equalled the downwind values. Upwind latent heat flux is set to 1 W m^{-2}, which is virtually equivalent to an infinitely large surface resistance, given that the available energy was at least two magnitudes larger. Upwind available energy is always assumed as 2/3 of downwind available energy. This crude estimate accounts, qualitatively, for three effects. First, the albedo upwind was probably somewhat higher than downwind, thus enhanced shortwave reflection reduced net radiation upwind. Second, the dry upwind surface must have been hotter than the wet downwind surface, leading to increased terrestrial longwave radiation. Third, we expect the soil heat flux of the dry surface to be a considerable fraction (perhaps of order of 30%) of the remaining net radiation.

To draw reference values for the upwind temperature and humidity from our measurements at 3.9 m, we employ two methods: one is to extrapolate them from downwind T, q, and their gradients in good fetch conditions. The other is to use T and q data at 3.9 m when winds were from the nearby stubble fields to the east, and to assume that these values were similar to those on the dry rangeland to the west. The two methods yield consistent results.

Downwind parameters are obtained as follows. Roughness length, z_0, is calculated from the log-linear wind profile (Garratt, 1992; p. 53), which gives $z_0 = z \exp(5z/L - k\bar{u}/u_*)$. Using k = 0.4 we obtain, on average, z_0 = 0.07 m. Results from 2.0 m and 3.9 m agree well. Surface resistance, r_s, is estimated as $r_s = (d + r_a F_d)/\lambda E$, where d is the linearized saturation deficit as defined in McNaughton and Laubach (1998), F_d its vertical flux, and $r_a = \bar{u}/u_*^2$ the aerodynamic resistance. The data scatter somewhat but agree reasonably between heights. We use the typical value of r_s = 30 s m^{-1} in the model runs. Lastly, downwind available energy is obtained from measurements of net radiation, soil heat flux, and water temperature.

The model results are evaluated at x = 447 m, which is the average fetch of the 42 selected experimental runs. Of the 15 model runs specified in Table AII, nine represent 'regular' runs, which cover the most common range of conditions. The other six are 'special' runs for less frequent conditions as indicated in the first column of the table. Two of the five runs with low u_* produce upward sensible heat fluxes, i.e., they fail to predict a stable IBL. They represent cases of 'weak' advection. We exclude them from further analysis because such cases did not occur in our experimental data. Two other model runs at low windspeed even fail to produce numerically stable solutions, for reasons not fully understood. We suspect

that this is due to our naive upper boundary condition (all properties at z = 150 m constant, i.e., equal to their upwind values at that height). These runs must be discarded too. This leaves 11 valid ones. For these, we give the stability parameter z/L (at z = 2.0 m) in the last column of the table. This is used in Figure 6 in the body of the paper.

References

Auble, D. L. and Meyers, T. P.: 1992, 'An Open Path, Fast Response Infrared Absorption Gas Analyzer for H_2O and CO_2', *Boundary-Layer Meteorol.* **59**, 243–256.

Bink, N. J.: 1996, *The Structure of the Atmospheric Surface Layer Subject to Local Advection*, Ph.D. Thesis, Wageningen Agricultural University.

Bland, W. L., Loew, J. T., and Norman, J. M.: 1996, 'Evaporation from Cranberry', *Agric. For. Meteorol.* **81**, 1–12.

De Bruin, H. A. R., Kohsiek, W., and van den Hurk, B. J. J. M.: 1993, 'A Verification of Some Methods to Determine the Fluxes of Momentum, Sensible Heat, and Water Vapour Using Standard Deviation and Structure Parameter of Scalar Meteorological Quantities', *Boundary-Layer Meteorol.* **63**, 231–257.

Foken, T., Weisensee, U., Kirtzel, H.-J., and Thiermann, V.: 1997, 'Comparison of New-Type Sonic Anemometers', in *Preprint Volume of the 12th Symposium on Boundary Layers and Turbulence, July 28–August 1, 1997, Vancouver, Canada*, American Meteorological Society, Boston, pp. 356–357.

Garratt, J. R.: 1992, *The Atmospheric Boundary Layer*, Cambridge University Press, U.K., 316 pp.

Hill, R. J.: 1989, 'Implications of Monin–Obukhov Similarity Theory for Scalar Quantities', *J. Atmos. Sci.* **46**, 2236–2244.

Jacobs, A. F. G., and McNaughton, K. G.: 1994, 'The Excess Temperature of a Rigid Fast-Response Thermometer and its Effects on Measured Heat Flux', *J. Atmos. Oceanic Tech.* **11**, 680–686.

Kaimal, J. C. and Finnigan, J. J.: 1994, *Atmospheric Boundary Layer Flows*, Oxford University Press, New York, 289 pp.

Kaimal, J. C., Wyngaard, J. C., Izumi, Y., and Coté, O. R.: 1972, 'Spectral Characteristics of Surface-Layer Turbulence', *Quart. J. Roy. Meteorol. Soc.* **98**, 563–589.

Katul, G. G., Albertson, J. D., Cheng-I Hseih, C. P. S., Sigmon, J. T., Parlange, M. B., and Knoerr, K. R.: 1996, 'The "Inactive" Eddy Motion and the Large-Scale Turbulent Pressure Fluctuations in the Dynamic Sublayer', *J. Atmos. Sci.* **53**, 2512–2524.

Lang, A. R. G., McNaughton, K. G., Chen, F., Bradley, E. F., and Ohtaki, E.: 1983, 'Inequality of Eddy Transfer Coefficients for Vertical Transport of Sensible and Latent Heats during Advective Inversions', *Boundary-Layer Meteorol.* **25**, 25–41.

Laubach, J. and McNaughton, K. G.: 1998, 'A Spectrum-Independent Procedure for Correcting Eddy Flux Measurements with Separated Sensors', *Boundary-Layer Meteorol.* **89**, 445–467.

McNaughton, K. G. and Jarvis, P. G.: 1983, 'Predicting Effects of Vegetation Changes on Transpiration and Evaporation', in T. T. Kozlowski (ed.), *Water Deficits and Plant Growth*, Academic Press, New York, pp. 1–47.

McNaughton, K. G. and Laubach, J.: 1998, 'Unsteadiness as a Cause of Non-Equality of Eddy Diffusivities for Heat and Vapour at the Base of an Advective Inversion', *Boundary-Layer Meteorol.* **88**, 479–504.

McNaughton, K. G. and Laubach, J.: 2000, 'Power Spectra and Cospectra for Wind and Scalars in a Disturbed Surface Layer at the Base of an Advective Inversion', *Boundary-Layer Meteorol.*, in press.

Moore, C. J.: 1986, 'Frequency Response Corrections for Eddy Correlation Systems', *Boundary-Layer Meteorol.* **37**, 17–35.

Oke, T. R.: 1987, *Boundary Layer Climates*, 2nd edn, Methuen Press, London, 435 pp.

Patankar, S. V.: 1980, *Numerical Heat Transfer and Fluid Flow*, Hemisphere, London, 197 pp.

Rao, K. S., Wyngaard, J. C., and Coté, O. R.: 1974, 'Local Advection of Momentum, Heat, and Moisture in Micrometeorology', *Boundary-Layer Meteorol.* **7**, 331–348.

Schotanus, P., Nieuwstadt, F. T. M., and de Bruin, H. A. R.: 1983, 'Temperature Measurement with a Sonic Anemometer and its Application to Heat and Moisture Fluxes', *Boundary-Layer Meteorol.* **26**, 81–93.

Townsend, A. A.: 1961, 'Equilibrium Layers and Wall Turbulence', *J. Fluid Mech.* **11**, 97–120.

Verma, S. B., Rosenberg, N. J., and Blad, B. L.: 1978, 'Turbulent Exchange Coefficients for Sensible Heat and Water Vapor under Advective Conditions', *J. Appl. Meteorol.* **17**, 330–338.

Vogt, R., Feigenwinter, C., Paw U, K. T., and Pitacco, A.: 1997, 'Intercomparison of Ultrasonic Anemometers', in *Preprint Volume of the 12th Symposium on Boundary Layers and Turbulence, July 28–August 1, Vancouver, Canada*, American Meteorological Society, Boston, pp. 354–355.

Webb, E. K., Pearman, G. I., and Leuning, R.: 1980, 'Correction of Flux Measurements for Density Effects Due To Heat and Water Vapour Transfer', *Quart. J. Roy. Meteorol. Soc.* **106**, 85–100.

Zermeño-González, A., and Hipps, L. E.: 1997, 'Downwind Evolution of Surface Fluxes over a Vegetated Surface during Local Advection of Heat and Saturation Deficit', *J. Hydrol.* **192**, 189–210.